SOME STUDIES ON SHORT OBLIQUE IMPINGING JETS

A Thesis Submitted
in Partial Fulfilment of the Requirements
for the Degree of
MASTER OF TECHNOLOGY

By
MUTHIAH PERUMAL

to the
DEPARTMENT OF CIVIL ENGINEERING
INDIAN INSTITUTE OF TECHNOLOGY, KANPUR
OCTOBER, 1978

CERTIFICATE

This is to certify that the thesis entitled "Some Studies on Short Oblique Impinging Jets" has been carried out under my supervision and the results embodied in this thesis have not been submitted to any other Institute or University for award of degree.

October , 1978

K. Subramanya.

(DR. K. SUBRAMANYA)
Professor
Department of Civil Engineering
Indian Institute of Technology, Kanpur

CE-1978-M-PER-Sem

ACKNOWLEDGEMENTS

I wish to express my grateful acknowledgements to Dr. K. Subramanya for suggesting this very interesting problem, for his supervision, suggestions, criticism and encouragement which was greatly responsible for the completion of my present work.

I am grateful to Dr. T. Gangadhariah for his useful suggestions and encouragement.

I am also grateful to Mr. Manuja and Mr. Gopalan, Research Engineers, Department of Electrical Engineering, I.I.T. Kanpur for their help in designing the Electronic Water Sensor.

I wish to express a deep sense of gratitude towards my friend Mr. K. Kumarasamy who encouraged me during various stages of this work.

Acknowledgements for friendly assistance and encouragement are also due to Messrs. R.Venkataraman,Lt.N.J.Seelan, Rakesh Chandra, Ramamurthy, Joy David, Khan and Porey.

Sincere thanks are due to Mr. Suresh Kumar, Mr. Satyanarayana and the staff of Hydraulics Laboratory for their help at various stages of experimental work.

Thanks are also due to Mr. V.K. Saxena and Mr. G.S. Trivedi for their excellent typing.

M. PERUMAL

TABLE OF CONTENTS

LIST OF FIGURES

LIST OF SYMBOLS

PART A

d	Nozzle exit diameter
H	Length of impingement
O	Geometric Centre of the circular plate . Also G.C.
P	Wall pressure in excess of ambient
P_s	Stagnation pressure
U_o	Nozzle exit velocity
P_*	Non-dimensionalised stagnation pressure
S	Stagnation point
r	Radial distance from S
r_p	Distance between stagnation point and the end of the impingement region.
r_{pc}	Approximate extent of the impingement region
s	Shift of S from O
θ	Polar angle
ϕ	Impingement angle
y	Space coordinate normal to wall
u	Radial velocity in the wall jet region in a vertical
u_m	Maximum velocity of u
β	Non-dimensionalised r
ν_a	Kinematic viscosity of air

R_o Nozzle Reynolds number

ρ_a Mass density of air

ρ_w Mass density of water

δ "One half" of wall jet thickness

δ_* "One half" radial distance of wall pressure

m A number

I.D. Inner Diameter

O.D. Outer Diameter

PART B

d Nozzle exit diameter

H Length of impingement

O Geometric centre of the circular plate. Also G.C.

P Wall pressure in excess of the hydrostatic pressure

P_s Stagnation pressure

U_o Nozzle exit velocity

u Mean radial velocity

S Stagnation point

r Radial distance from S

s Shift from O

θ Polar angle

ϕ Impingement angle

y Space co-ordinate normal to wall

$d\theta$	Smaller angle θ
β	Non-dimensionalised r in the impingement region
α	Non-dimensionalised r in the radial flow region
ν_w	Kinematic viscosity of water
R_o	Nozzle Reynolds number
Q	Nozzle discharge
ρ_w	Mass density of water
δ_*	"One half" radial distance of wall pressure
r_*	"One half" radial distance of mean velocity
q	Discharge in a $d\theta$ angle segment
$\sum_{\theta} q$	Discharge in the θ segment

ABSTRACT

Name of student	:	M. Perumal
Programme	:	M. Tech.
Department	:	Civil Engineering
Title of thesis	:	SOME STUDIES ON SHORT OBLIQUE IMPINGING JETS
Thesis supervisor	:	Dr. K. Subramanya

The oblique impingement of circular short submerged jet and free flow jet on smooth wall have been studied experimentally. The earlier work considered the study of short jet impingement for the impingement angle, $\phi = 45°$. So the present study is carried out for angle, $\phi=60°$ to fill some gap of information left by earlier investigator. Also an exploratory study on free flow jet impingement has been done to know the behaviour of flow after impingement on the solid surface.

It has been found in the present study of short submerged jet impingement that velocity characteristics in the wall jet region are not at all affected by the nature of impingement confirming the results of the previous study with $\phi = 45°$. On the other hand, wall pressure characteristics not only affected by the nature of impingement but also affected by the change of ϕ, except the pressure similarity characteristics.

The exploratory study on oblique impinging free flow jet reveals that the similarity pressure profile of the impingement region is exactly same as in the case of submerged jet impingement. However, length scale differs for each other. A empirical equation is developed to predict mean velocity at any radial distance from the stagnation point. The variation of discharge along the circumferential direction has also been studied.

CHAPTER 1

INTRODUCTION

1.1 Introduction:

The impingement of turbulent jets on solid surfaces finds application in several engineering problems such as jets issuing from hydraulic outlet works, weirs, vertical take-off aircrafts, various spraying devices and in chemical industries. The angle at which the jet impinges the surface may vary between 0° and 90°. According to the type of flow situations there are two types of jets. They are 1. submerged jet and 2. free flow jet.

1. Submerged jet: A jet can be called as a submerged jet if it travels through a medium having essentially the same fluid characteristics of that issuing jet medium. Examples are air jet in air, water jet in water etc.

2. Free flow jet: A jet is defined as a free flow jet where a heavy fluid flows in a very light fluid medium giving rise to very high gravity effects. For example water jet in Air.

1.2 Part A :

Oblique impingement of short submerged jet (Air jet in air).

1.2.1 Description of the experimental study:

Consider a circular submerged jet impinging at an angle of ϕ , as shown in Figure 1.1(a). The jet is formed by a nozzle of diameter, d with nozzle exit velocity, U_o. The length of impingement H is defined to be the distance from the nozzle to the wall along the jet centre line. The acute angle between the jet centre line projection and the plane solid surface is defined as the impingement angle. The jet nozzle is so adjusted that jet centre line coincides with the geometric centre, O of the circular plate on which it impinges.

Three types of flow regions are present. The free jet region extends from the point where the jet issues to some distance above the wall. In the impingement region the wall pressure P is above that of ambient. The stagnation pressure, P_s does not occur at O . Instead it is removed by a distance, s from O along the 0°-180° line. The impingement region ends at a distance r_p from the stagnation point, S where the pressure is same as that of ambient. From there

the wall jet region starts having decreasing energy and velocity with the growth of wall jet thickness. The cylindrical system (r, θ , y) with the origin at the stagnation point, S is used to describe the different flow regions.

Depending upon the length of impingement, the jet can be defined as long jet or short jet.

Long jet: The jet can be defined as long jet if it gets fully developed before impingement. Jet with length of impingement $H > 15.0$ d is considered to be a long jet.

Short jet: The jet can be defined as short jet if it does not get fully developed before impingement. Jet with length of impingement $H \leq 15.0$ d is considered as short jet.

1.2.2 Present Work:

The present investigation is aimed at providing further information on the behaviour of oblique impinging short jet with $\emptyset=60°$. The following details were studied:

a. The velocity distribution in the wall jet region and

b. The wall pressure distribution in the impingement region.

Further details on this study are present in Part A.

1.3 Part B:

Oblique impingement of free flow jet (water jet in air).

1.3.1 Description of the experimental study:

Figure 1.2(a) shows water jet issuing from a nozzle of diameter, d with nozzle exit velocity, U_o impinging at an angle, $\emptyset$ on a circular plate after travelling through the medium of air. To distinguish from the previous case it is called free flow jet.

There are mainly three regions of flow. They are 1. Pre-impingement region , 2. Impingement region and 3. Radial flow region.

Pre-impingement region extends from the point where the jet issues to some distance above the wall. In the impingement region the wall pressure P is above that of corresponding hydrostatic pressure. Radial flow region starts immediately after the impingement region. The flow can be either supercritical or subcritical. Transition from supercritical flow to subcritical flow will take place through hydraulic jump depending upon the downstream conditions.

The definition of long jet and short jet used in the submerged jet study cannot be applied for free flow jet study since the jet splits up for increasing impingement length due to the effects of gravity and air entrainment.

1.3.2 Present work:

The present work is an exploratory study to determine the essential characteristics of impingement region and the radial flow region. The following details were studied.

a. The wall pressure distribution in the impingement region and finding, if any, correspondence with that of submerged jet.

b. The mean velocity distribution in the radial flow region.

c. The discharge variation in $\theta = 0° - 180°$ range.

Further details on this study are present in Part B.

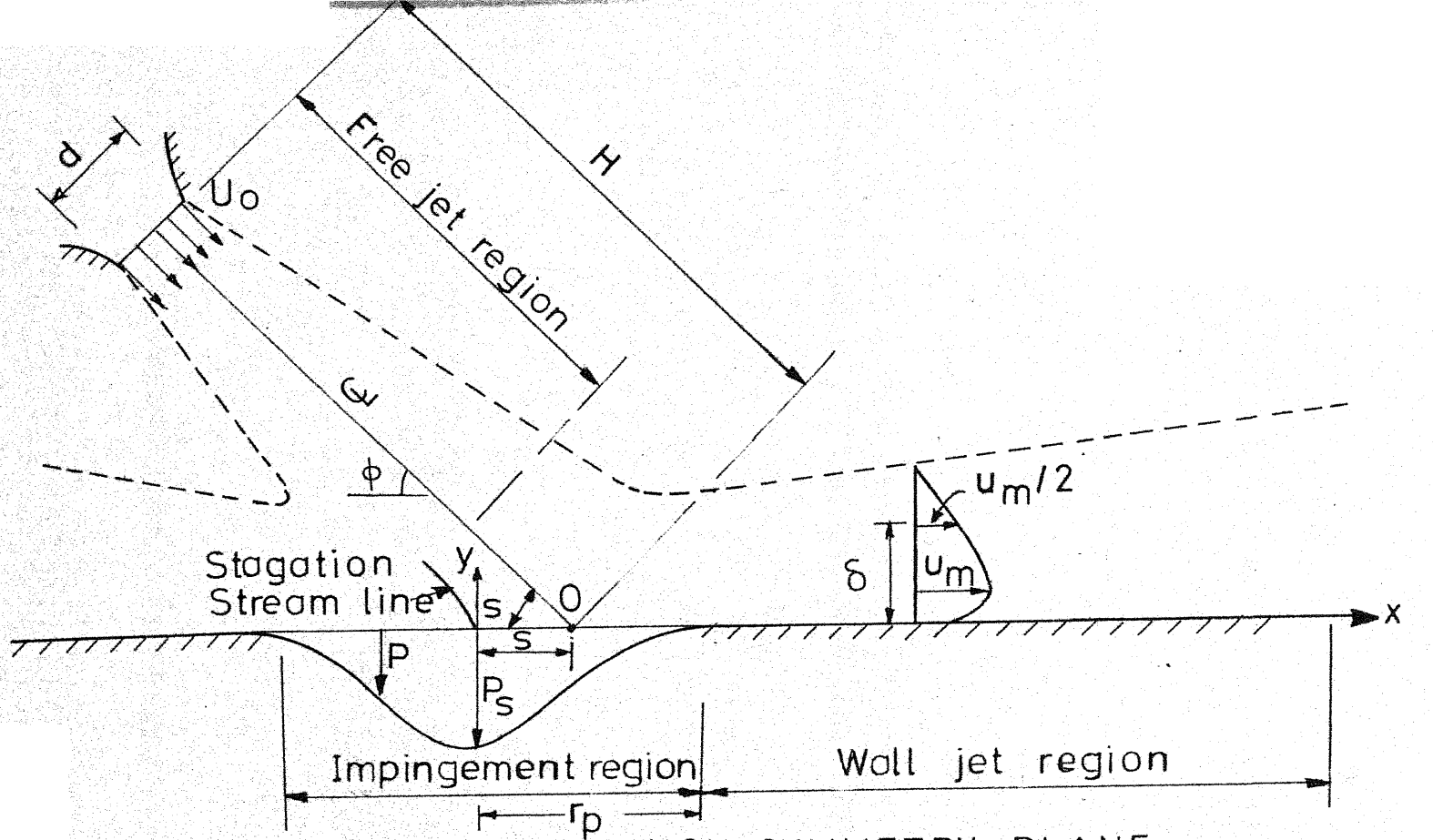

(a) SECTION THROUGH SYMMETRY PLANE

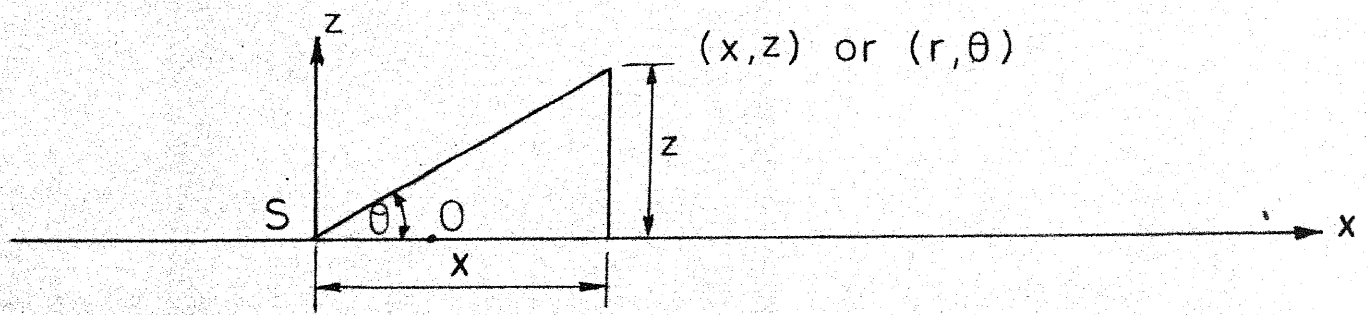

(b) PLAN VIEW

FIGURE 1-1 DEFINITION SKETCH (Submerged jet impingement)

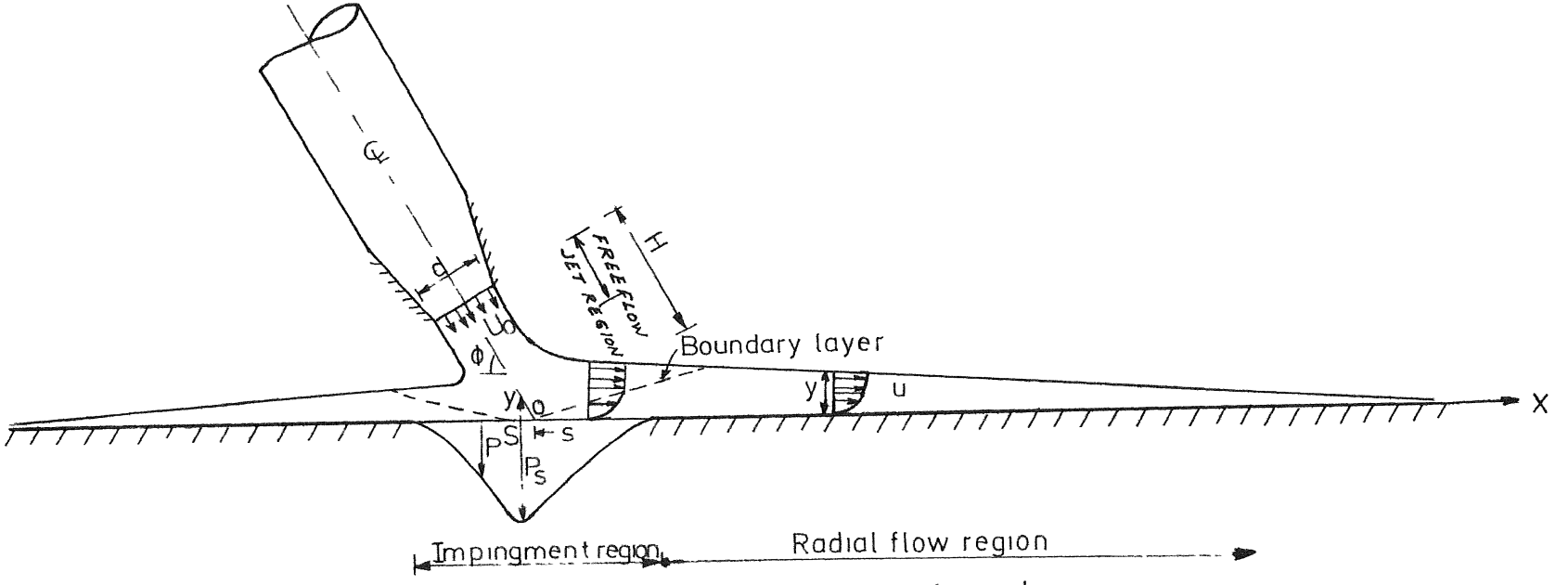

(a) Section through symmetry plane

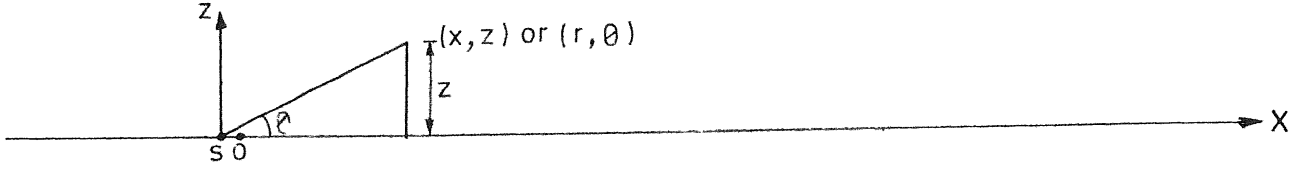

(b) Plan view

FIGURE 1·2 DEFINITION SKETCH (Free flow jet impingement)

PART A

OBLIQUE IMPINGEMENT OF SHORT SUBMERGED JET (Air jet in Air)

CHAPTER 2

LITERATURE REVIEW

2.1 Air Jet In Air :

While literature available in the case of vertical impinging jets are plenty, there are very few works on topics related to oblique impinging jets. Abramovich (1), Rajaratnam (10) and others (5,6) have studied the behaviour of circular turbulent impinging jets. In oblique impingement, except in the free jet region, the flow is not totally axisymmetrical as in the case of normal impingement. The flow will be three dimensional elsewhere and therefore the oblique impingement problem represents a considerable geometrical generalization.

In studies on radial wall jets, the wall jet region has been extensively studied both analytically and experimentally.

Naib (7) has presented an experimental study of the wall jet region with zero length of impingement. This study was restricted to observations of velocity and jet thickness on the plane of symmetry and some velocity measurements for evaluating the lateral spreading near the wall.

Beltaos (3) has studied in detail the effects of oblique impingement of long submerged jet, in the impingement region and in the wall jet region. He has carried out experiments by varying the length of impingement, H from 15d to 47d and has studied the velocity profile observation in the wall jet region and wall pressure distribution in the impingement region.

He developed a semi-empirical method to predict wall pressure in the impingement region and theory for prediction of flow properties in the wall jet region. The thickness of the wall jet was found to grow linearly on any radial line for any impingement angle at a universal slope which is equal to 0.0755. Also he showed that $\frac{U_o}{u_m} = A\ (r/d)$, where u_m is the maximum radial velocity component in a section considered at any radial distance r, from the stagnation point S, and A, the proportionality constant which depends on ϕ and θ.

There are many practical engineering problems in which the length of impingement, H may be less than 15d. Beltaos (3) considered these oblique impingement of short jets as belonging to a different class of problem.

Recently Sinha (11) has studied oblique impingement of short jet with $\phi = 45°$ and length of impingement varying from 1d to 10d. The salient features of his studies are follows :

a. Wall jet region investigation :

The velocity similarity profile is same as obtained by Beltaos (3) for long jets with impingement angle $\phi = 20°$, $30°$, $45°$ and $60°$. Also the growth of wall jet is found to be linear with the proportionality constant being as same as in the case of long jet impingement obtained by Beltaos (3). Also the relationship between U_o/u_m and r/d is found to be similar as in the case of long jet impingement and can be expressed as $U_o/u_m = m\ (r/d)$ where m is a function of ϕ and θ. The m values obtained in Sinha's (11) experiments are given below.

S.No.	Polar angle	Sinha's (11) m	Beltaos's (3) m
1	0	0.38	0.39
2	45	0.60	-
3	90	1.29	-
4	135	1.29	-

Also he found at $r \geq 5.0d$ the wall jet is fully developed for all values of H/d tested.

b. Impingement region investigation :

Sinha (11) obtained a semi-empirical relationship for the pressure similarity profile as $P/P_s = \exp(-0.693\beta^2)$ which was obtained by Beltaos (3) also for the case of long jets. But Sinha (11) found the effect of impingement of short jet on the criteria of location of stagnation point and magnitude of stagnation pressure differs remarkably from that of long jet impingement.

Sinha (11) concludes that short jet impingement affects only the impingement region in certain characteristics and the wall jet behaviour is same as that of classical wall jet.

CHAPTER 3

EXPERIMENTAL DETAILS

3.1 Experimental Investigation :

In the present investigation the details of oblique impingement of circular jets with length of impingement, $H < 15.0\ d$ were aimed for studies. Due to the time restriction only one value of the angle of impingement, was studied i.e. ϕ was kept constant at 60°. Air was used as the working medium, as it was found to be convenient to study the various parameters with least effort. Air was supplied by a blower (1 H.P. and 2800 R.P.M.) with controlled air inlet and through a large size (90 mm) hose which acted as plenum chamber. Two nozzles of internal exit diameter, $d = 12.7$ mm and 25.4 mm were used in the study. The nozzle exit velocity, U_o was kept below 90 m/sec. in order to avoid the compressibility effects. The nozzle Reynold's number, $R_o = \frac{U_o\, d}{\nu_a}$ (ν_a = kinematic viscosity) was varied between 30,000 and 95,000 and the relative impingement length, H was in the range of 2.0d to 10.0d.

A total number of 13 experiments were conducted and their particulars are summarized in Table 1.

TABLE 1

DETAILS OF EXPERIMENT

Angle of Impingement, $\phi = 60°$

Barometric Pressure = 72 cms (Average) of mercury

Temperature Range 31°C - 36°C

Kinematic Viscosity of air, $\nu_a = 1.5 \times 10^{-5} m^2/sec.$ (at 20°C)

S. No.	Run No.	Diameter of Nozzle, d mm	H/d	Nozzle Exit Velocity, U_o m/sec.	Reynold's No. $R_o = \frac{U_o d}{\nu_a}$
1	1(A)	25.4	2.0	52.0	88,055
2	1(B)	25.4	2.0	36.8	62,315
3	2(A)	25.4	4.0	52.0	88,055
4	2(B)	25.4	4.0	36.9	62,485
5	3(A)	25.4	6.0	55.7	94,320
6	3(B)	25.4	6.0	39.4	66,720
7	4(A)	25.4	8.0	51.8	87,715
8	4(B)	25.4	8.0	36.6	61,975
9	5(A)	25.4	10.0	52.0	88,055
10	5(B)	25.4	10.0	36.8	62,315
11	6(C)	12.7	8.0	51.8	43,860
12	6(D)	12.7	8.0	36.6	30,990
13	7(C)	12.7	4.0	52.0	44,025

3.2 Experimental Set-up :

The experimental set-up used in the study is shown in Figure 3.1. A table was made with angle irons over which an aluminium plate was mounted. At the centre, a circular smooth aluminium plate cutout of diameter 600 mm was placed such that it could be rotated in the circumferential direction about its centre. The circular cutout was devided at 15° polar angle intervals and distances in centimeter were marked from geometric centre, O, on each radial line for measurement purposes. On two of the radial lines, which are perpendicular to each other, 1.6 mm static pressure taps were located for wall pressure measurements. The first 7 taps in one of those radial lines were placed at 1 cm apart and the rest at 2 cm apart from the centre, O. The pressure taps in the other radial line were so located to measure the in between pressures of the previous radial line pressure tap measurements.

3.3 Measurements :

The radial wall pressure distribution were obtained at 15° polar angle increments by using static pressure taps in the cutout. Two MAGNEHELIC type of pressure gauges (made by Dwyer and Co., U.S.A.) in the range of 0-2 inch

and 0-0.5 inch of water and a water filled vertical U-tube manometer were used for measurement purposes. Using these, the contours of different pressure intensity like P/P_s = 0.9, 0.8, 0.5 etc. could be plotted for each run.

3.4 A Typical Experiment :

Firstly, the temperature, t°C and barometric pressure in cm of mercury of the ambient at the set-up were noted. The nozzle was fixed at an angle, ϕ of 60° and at the fixed length of impingement, H-say = 2d. Then the blower was started and the velocity, U_o at the nozzle exit was adjusted by controlling the blower inlet.

The run was started with wall pressure measurements. The pressure taps were connected to Magnehelic pressure gauges or to the U-tube manometer depending upon the range of pressure and the pressures were noted. Due to the symmetry of flow only one half portion of the plate was considered for observations i.e. readings were taken in between 0° to 180° of polar angle, θ. Wall pressure readings were taken at 15° interval and on each radial line pressure taps readings were noted until the reading shows the ambient value.

The velocity observations were recorded with total head tube which has a hypodermic tube of size 1.25 mm O.D. and 1.00 mm I.D. The total head tube was connected to a vernier attachment which can be moved up and down with an accuracy of 0.1 mm Observations were taken at 4-radial lines i.e. on $\theta = 0°$, $45°$, $90°$ and $135°$ and at intervals of 2d to 3d. Thus in a radial line 4 or 5 vertical sections were considered for velocity measurements. In each section velocity readings were taken at 1 mm or 2 mm interval depending upon the thickness of the wall jet.

Thus about 1100 readings were taken for wall pressure calculations and about 1150 readings were taken for velocity calculations in all runs.

All the measurements were conducted at co-ordinate positions determined with reference to the geometrical centre of the plate due to its easy location. However, for analysis purposes they were converted to the co-ordinates with stagnation point, S as the origin. The error involved in this is believed to be negligible because the location of stagnation point was not very much removed from geometrical centre, O, in all the runs.

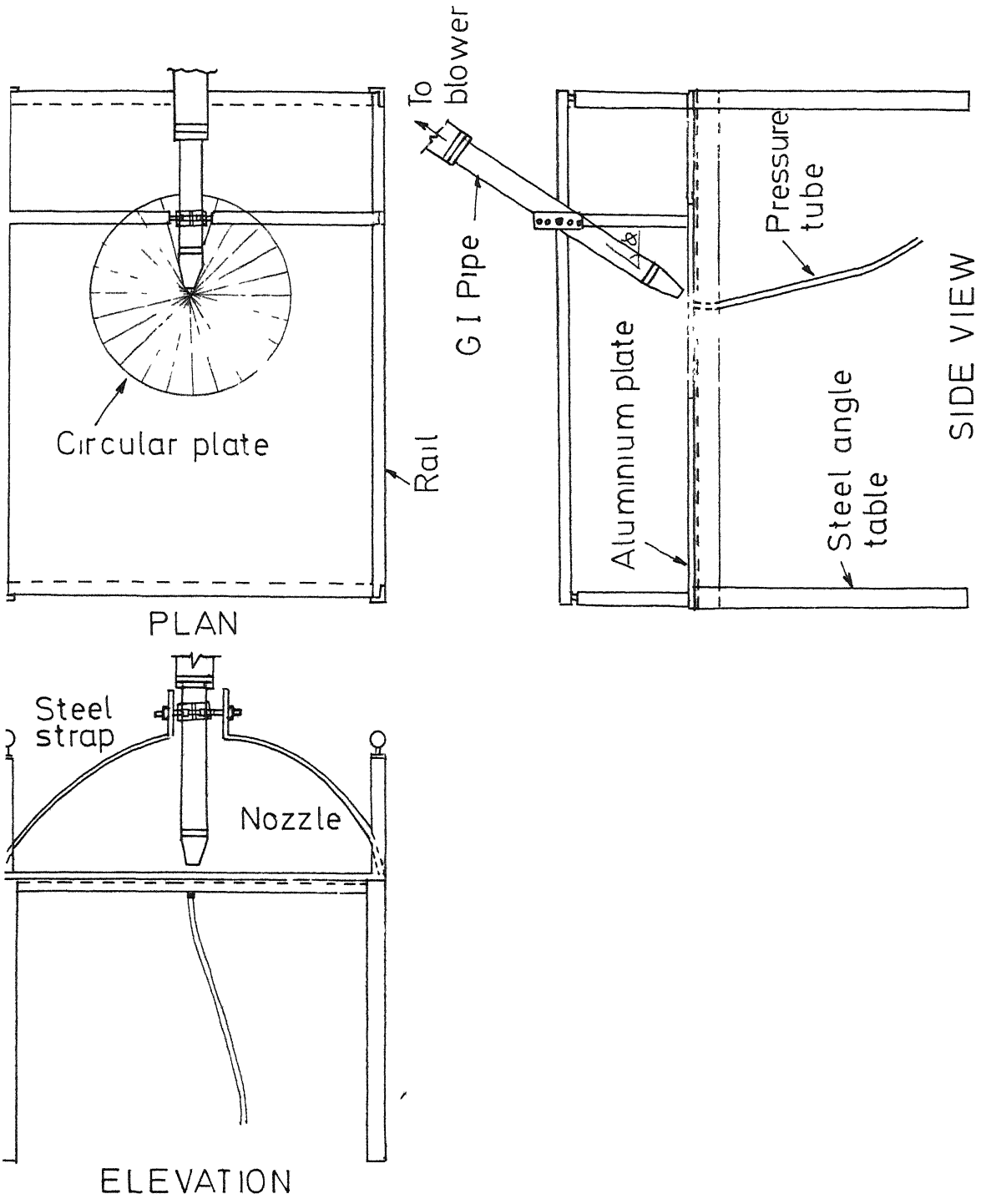

FIGURE 3.1 SCHEMATIC DIAGRAM OF EXPERIMENTAL SET-UP

CHAPTER 4

ANALYSIS AND DISCUSSION

The data collected in the investigation were analysed to study wall jet and impingement regions, taking the following in detail.

4.1 Velocity Profile Observations:

Initially, velocity head was measured in terms of head of water at different radial locations and then they were converted into velocity, u, by using the formula

$$u = \sqrt{2g \left(\frac{\rho_w}{\rho_a}\right) h_w}$$

where, ρ_a = mass density of air at temperature t°C of experiments in kg/m^3, ρ_w = mass density of water at temperature t°C in kg/m^3 and u = the radial component velocity of air in m/sec.

4.1.1 Similarity plot:

To test the similarity of velocity profiles in the wall jet region, for each location (r, θ), similarity plot between u/u_m and y/δ , where u_m is the maximum radial component velocity and δ is the larger value of y

where u/u_m =0.5, were plotted. (See Figures 4.1, 4.2a, 4.2b and 4.2c). In Figure 4.1 u/u_m has been plotted for d=25.4 mm, θ =0°, 45°, 90° and 135° and H/d = 2.0. It is seen that all the data lie on a single curve (curve A) irrespective of the values of U_o, r/d. The same curve A has also been obtained for d = 25.4 mm with H/d = 4.0 (See Figures 4.2a and 4.2b) in the different ranges of nozzle exit velocity, U_o and for d = 12.7 mm with H/d = 4.0 (See Figure 4.2c), at θ = 0, 45°, 90° and 135°. Similarly it is found all the other data also lie on the same curve A. Hence the data confirms the existence of similarity in velocity profiles in the wall jet region i.e. non-dimensional velocity u/u_m is independent of ϕ, d, H/d, θ and r/d for r/d > 3.0 . This has been reported by Beltaos (3) and Sinha (11) . Further the curve A is found to be the same as the classical wall jet curve. From these plots (See Figures 4.1, 4.2a, 4.2b and 4.2c) it is found that the fully developed wall jet commences at around $r = r_{pc}$ = 7.0 d. For $r < r_{pc}$ the flow can be in the impingement region or in the developing region of wall jet.

4.1.2 Scales:

The scales of the above similarity plot are length scale, δ and velocity scale, u_m.

4.1.2.1 Length scale, δ :

The length scale can be expected to depend in general as;

$$\delta = fn\ (\ r,\ H\ ,\theta\ ,\ \phi\ ,\ d\ )$$

Hence $$\frac{\delta}{H} = fn\ (\ \frac{r}{H}\ ,\ \theta\ ,\ \frac{H}{d}\ ,\ \phi\ )$$

In the present study ϕ = constant = 60°. A plot between δ /H and r/H has been plotted in Figure 4.3. It is seen that the resulting plot is independent of θ and H/d for the given value of ϕ. It is found that δ /H varies linearly with r/H and a straight line originating from origin is obtained. The equation of the best fit line is δ = 0.0760 r . This agrees well with the results of Beltaos (3) (δ = 0.0755 r) and of Sinha (11) (δ = 0.0750 r) . It is interesting to note that this value is exactly the same as the growth rate of a axisymmetrical radial wall jet reported by Bakke (2).

Thus it is seen that δ /r = 0.076 and is independent of ϕ, θ and H/d for both long and short jets.

4.1.2.2 Velocity scale, u_m:

The velocity scale can be expected to depend upon:

$$u_m = fn\ (U_o,\ r\ ,\ d,\ \theta\ ,\ \phi,\ H\ )$$

hence, $\frac{U_o}{u_m}$ = fn (r/d, θ , H/d , ∅)

A plot between U_o/u_m and r/d is shown in Figure 4.4. It is seen that for constant value of ∅ , U_o/u_m is independent of H/d but is dependent on r/d and θ. A linear variation has been obtained for different values of r/d, which could be expressed as $\frac{U_o}{u_m}$ = m (r/d) where m is a function of θ. Variation of m with θ has been shown in Figure 4.5 and results are given in Table 2. The results obtained are in general agreement with the Beltaos's (3) results.

TABLE - 2

DETAILS OF 'm'

S.No.	Polar Angle θ°	Value of 'm'	Beltaos's (3) 'm'
1	0	0.466	0.510
2	45	0.609	-
3	90	0.976	0.933
4	135	1.360	-

In Figure 4.5 , data of Sinha (11) for $\phi = 45°$ is also plotted. It is observed that his data is also in general agreement with the present data indicating that m is a very weak function of ϕ in this range.

From the above study of wall jet velocity distribution characteristics it is evident that velocity characteristics are independent of nature of impingement i.e. whether the jet is under-developed (short) or fully-developed (long).

4.2 Wall Pressure Observations:

In the impingement region the observed wall pressures are used to plot equal pressure contours. Typical wall pressure contours are shown in Figures 4.6a, 4.6b, 4.6c and 4.6d. From these it is seen that the contour shapes deviate from the circular pattern of normal impingement. Also, the maximum wall pressure i.e. stagnation pressure, P_s does not occur at the geometrical centre, O but is shifted by a distance, s upstream of O and along the $\theta = 0^o - 180^o$ line.

4.2.1 Stagnation pressure:

The variation of stagnation pressure, P_s with respect to H/d is shown in Figure 4.7. It is seen from

this plot of $P_* = P_s/(\frac{\rho_a U_o^2}{2})$ and H/d, that the stagnation pressure is a strong function of length of impingement, H. Stagnation pressure data are given in Appendix A-2. For the fully developed impinging jets, Beltaos (3) obtained

$$\frac{P_s}{(\rho_a U_o^2/2)} \left(\frac{H}{d}\right)^2 = K = fn\ (\phi) \qquad \text{(Eq. 1)}$$

For $\phi = 60°$, K was found to be = 40. In the present case suitable extrapolation of the plot P_* vs. H/d passes through the point, obtained by Eq. 1. Corresponding to H = 15.5 d and $\phi = 60°$. Comparison with Sinha's (11) data shown in Figure 4.7 indicates that P_* is a function of ϕ also.

4.2.2 Location of stagnation point:

A plot between s/H and H/d is shown in Figure 4.8. It is clear that maximum value of s/d occurs when H/d is very small and decreases as H/d increases. For long jets Beltaos (3) obtained a constant value of s/H = 0.03. In the Figure 4.8 a likely variation of s/H with H/d is shown by a smooth curve approaching the corresponding constant value of Beltaos (3) at H/d = 15.0. In the present case the

stagnation point was determined by tracing the contour of equal pressure and as such the location was subjective. In view of the small values of s/H involved, the scatter of the data is not too severe.

4.2.3 Similarity of pressure profile:

A non-dimensional pressure profile is plotted for each run in order to know the behaviour of pressure distribution in radial direction (See Figures 4.9a and 4.9b). This plot is between P/P_s and $r/\delta*$, where P is the wall pressure at any radial distance r about θ, P_s is the stagnation pressure and $\delta*$ is the value of r at which $\frac{P}{P_s} = 0.5$. This plot is found to be independent of ϕ, θ and H/d. The obtained curve is of Gaussian function type and can be expressed as

$$\frac{P}{P_s} = \exp (- 0.693 \beta^2), \text{ where } \beta = r/\delta*$$

This agrees well with the similar results obtained by Beltaos (3) and Sinha (11).

4.2.4 Variation of length scale, $\delta*$:

The length scale $\delta*$ i.e. the value of r at $P/P_s = 0.5$ is studied by a plot between $\delta*/H$ and H/d as shown in

Figure 4.10 . It is seen that $\delta*/H$ is dependent on θ .

The study of the impingement region shows that the wall pressure distribution is similar and the similarity profile is same for both long and short jets and is independent of ϕ. However, the scales of this similarity plot viz. $\delta*$ and P_s are different for short jets. The stagnation pressure P_s and its location S are function of H/d and ϕ for short jets.

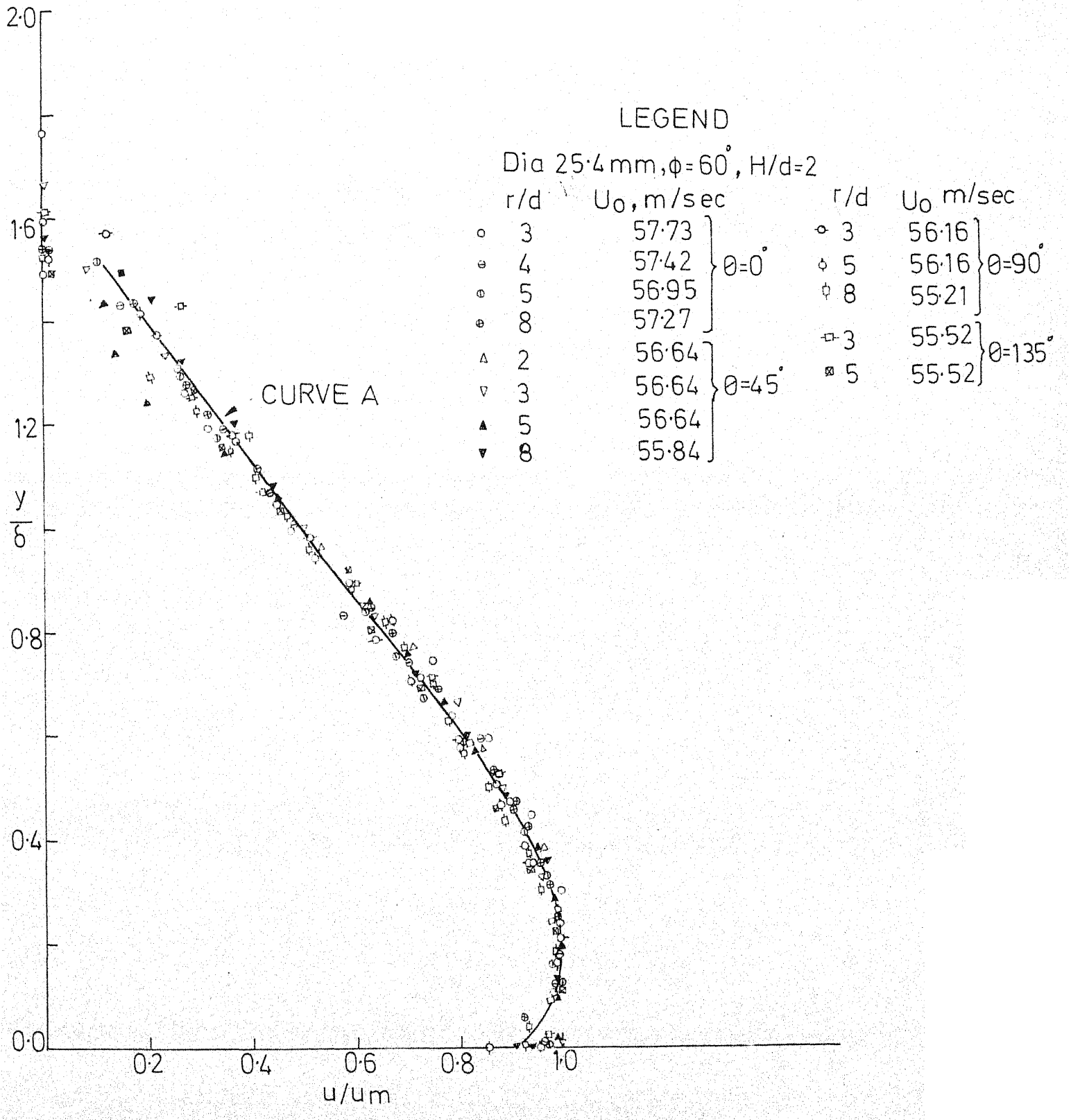

FIGURE 4·1 SIMILARITY OF RADIAL VELOCITY (Wall jet region)

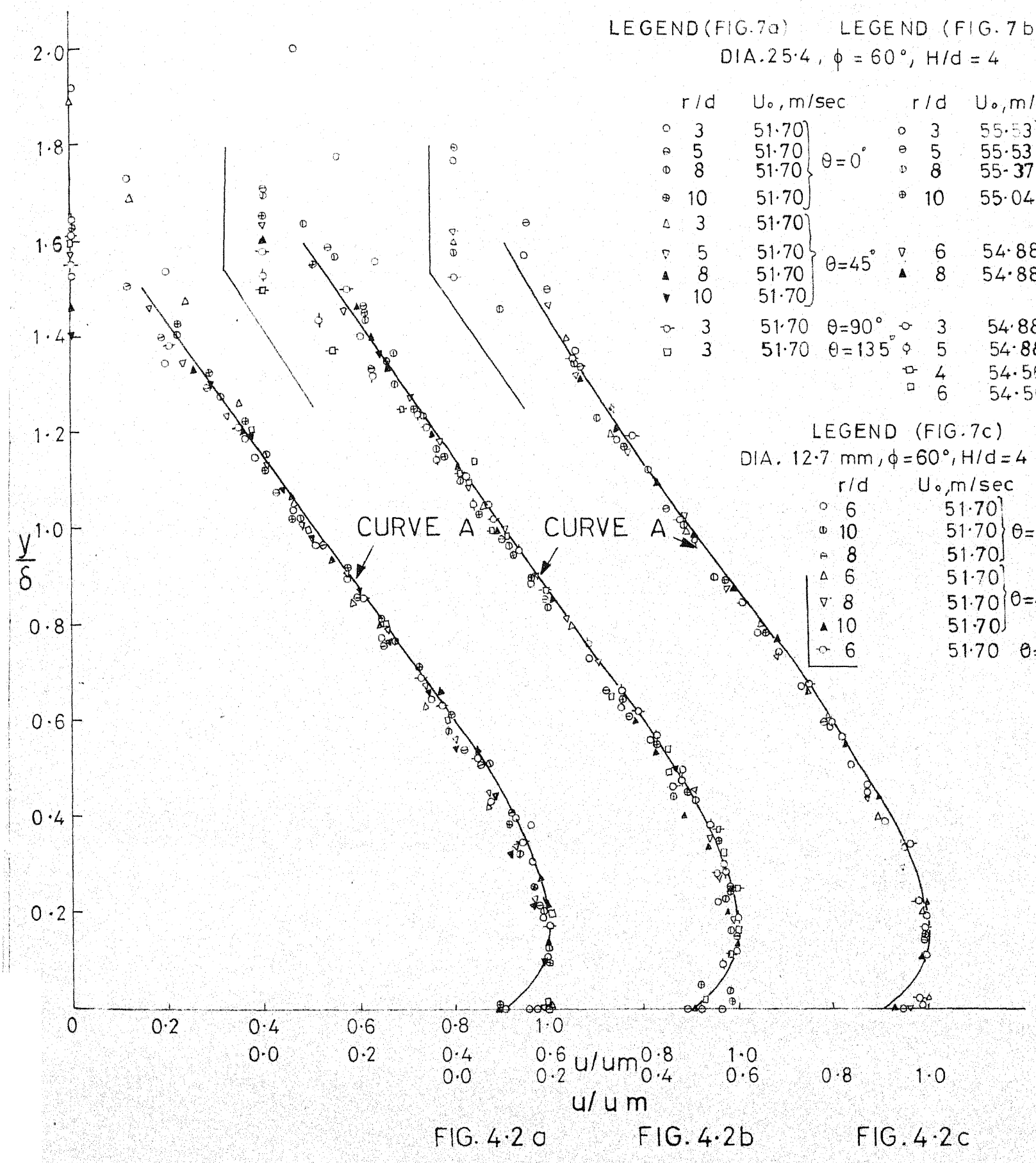

FIG. 4·2 a FIG. 4·2 b FIG. 4·2 c

FIGURE 4·2 SIMILARITY OF RADIAL VELOCITY (Wall Jet Region)

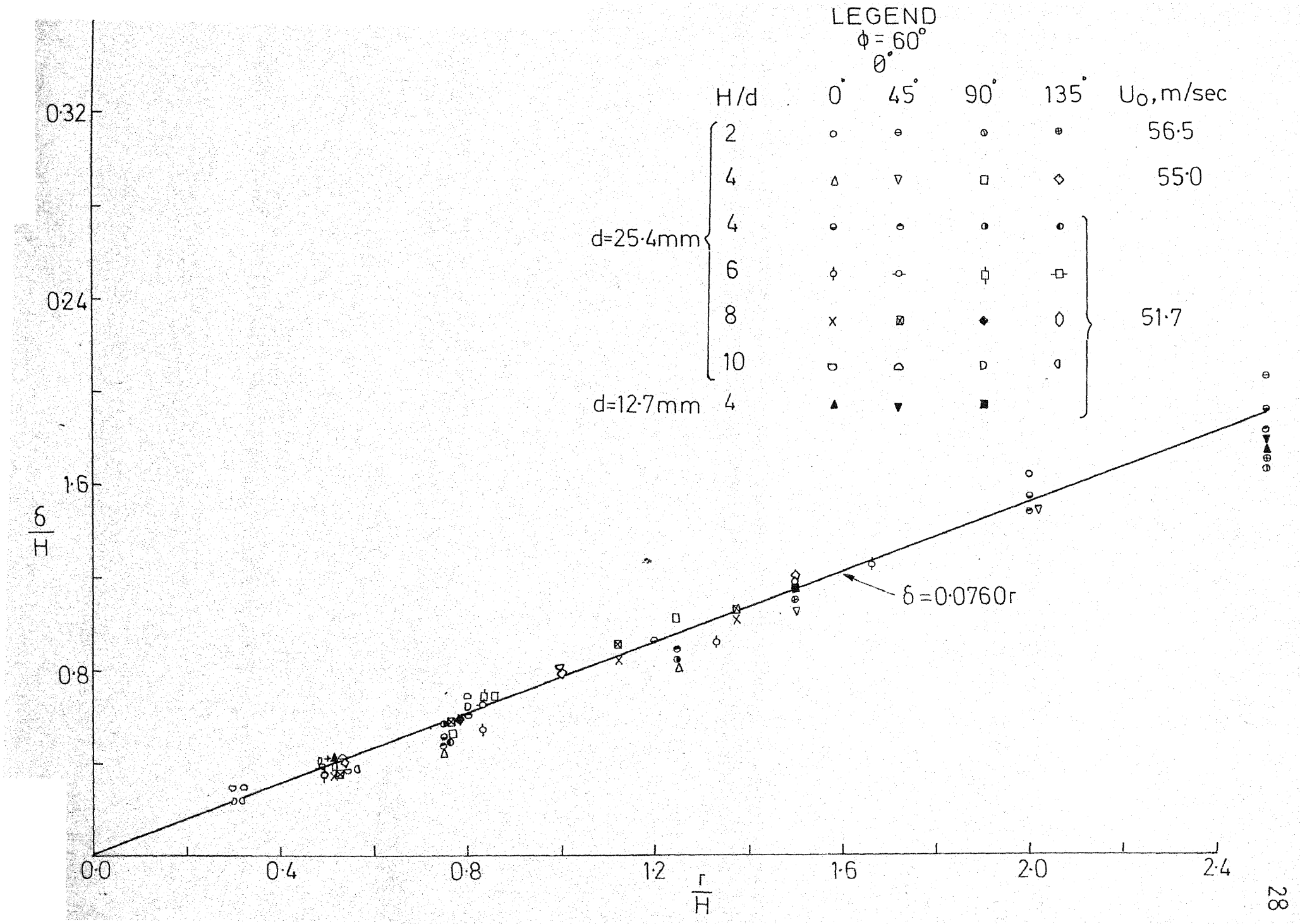

FIGURE 4·3 LENGTH SCALE, δ

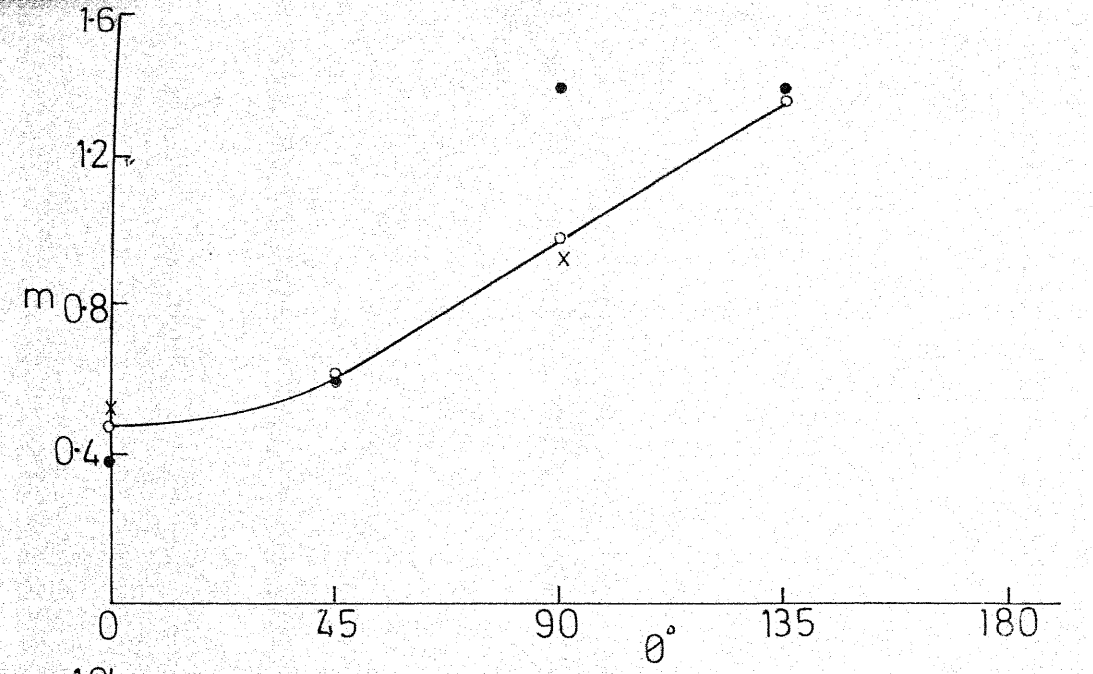

LEGEND
- o - PRESENT WORK
- x - BELTAOS'S ($\phi = 60^\circ$)
- • - SINHA'S ($\phi = 45^\circ$)

FIGURE 4·5 VARIATION OF m

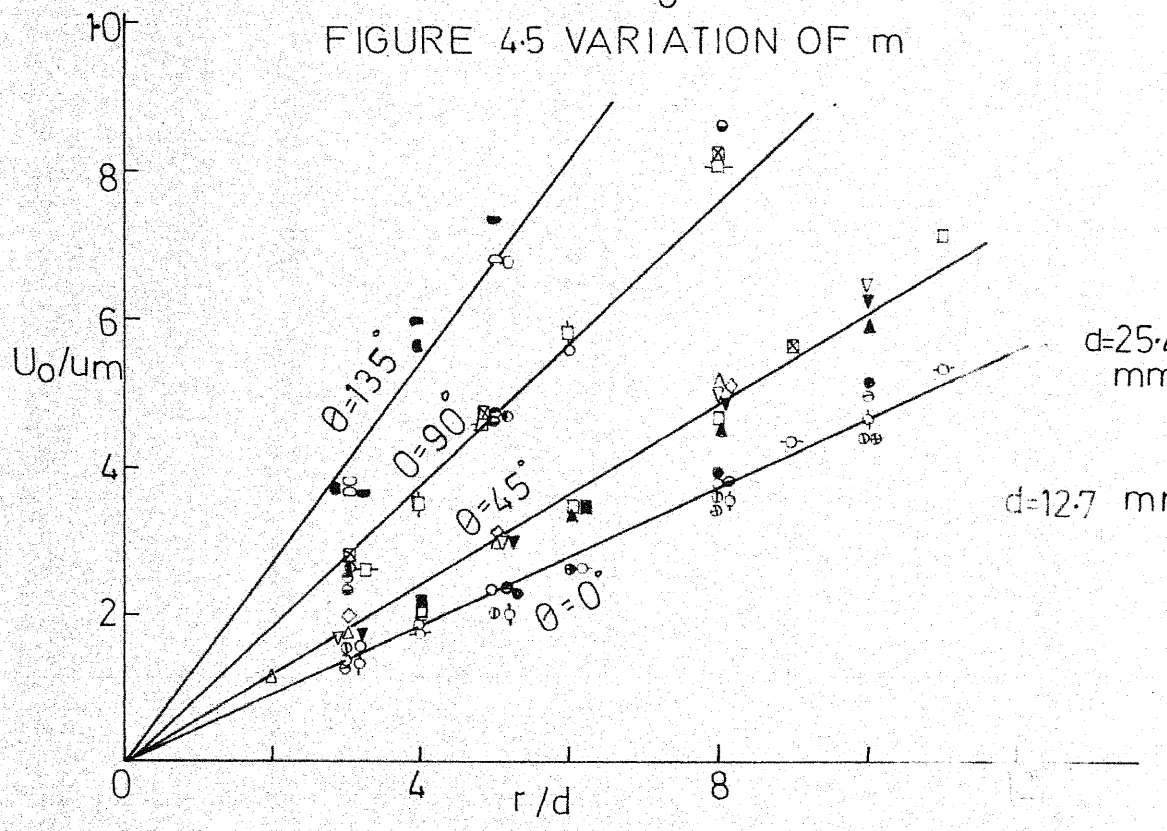

LEGEND
$\Phi = 60^\circ$

H/d	θ = 0°	45°	90°	135°
2	○	△	○	○
4	⊖	▽	⊖	⊖
6	◐	□	◐	◐
6	⊕	▼	⊕	⊕
8	⊖	■	⊕	■
10	●	◇	⊠	⊠
4	⊕	▲	●	

FIGURE 4·4 VELOCITY SCALE um

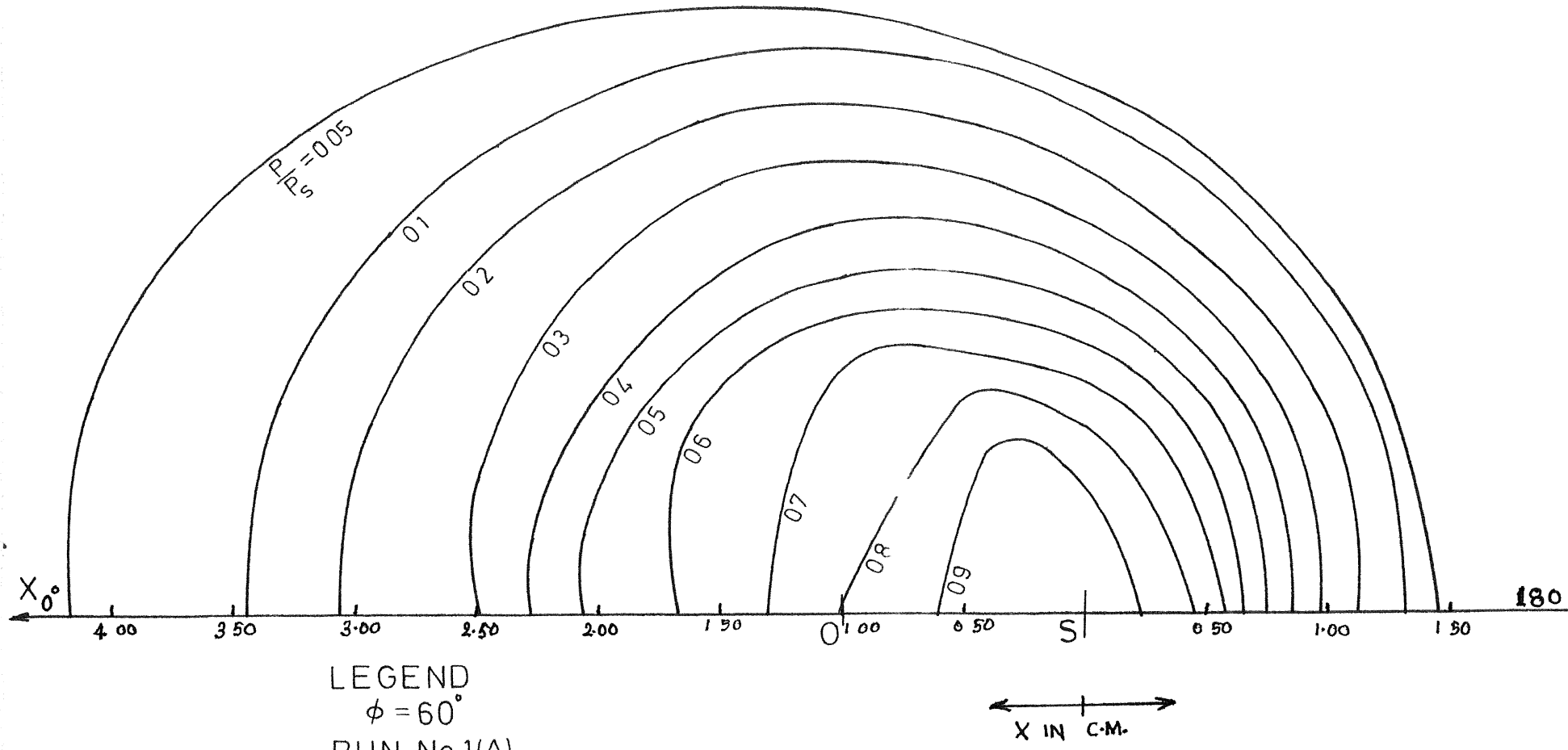

FIGURE 4·6 a PRESSURE CONTOURS

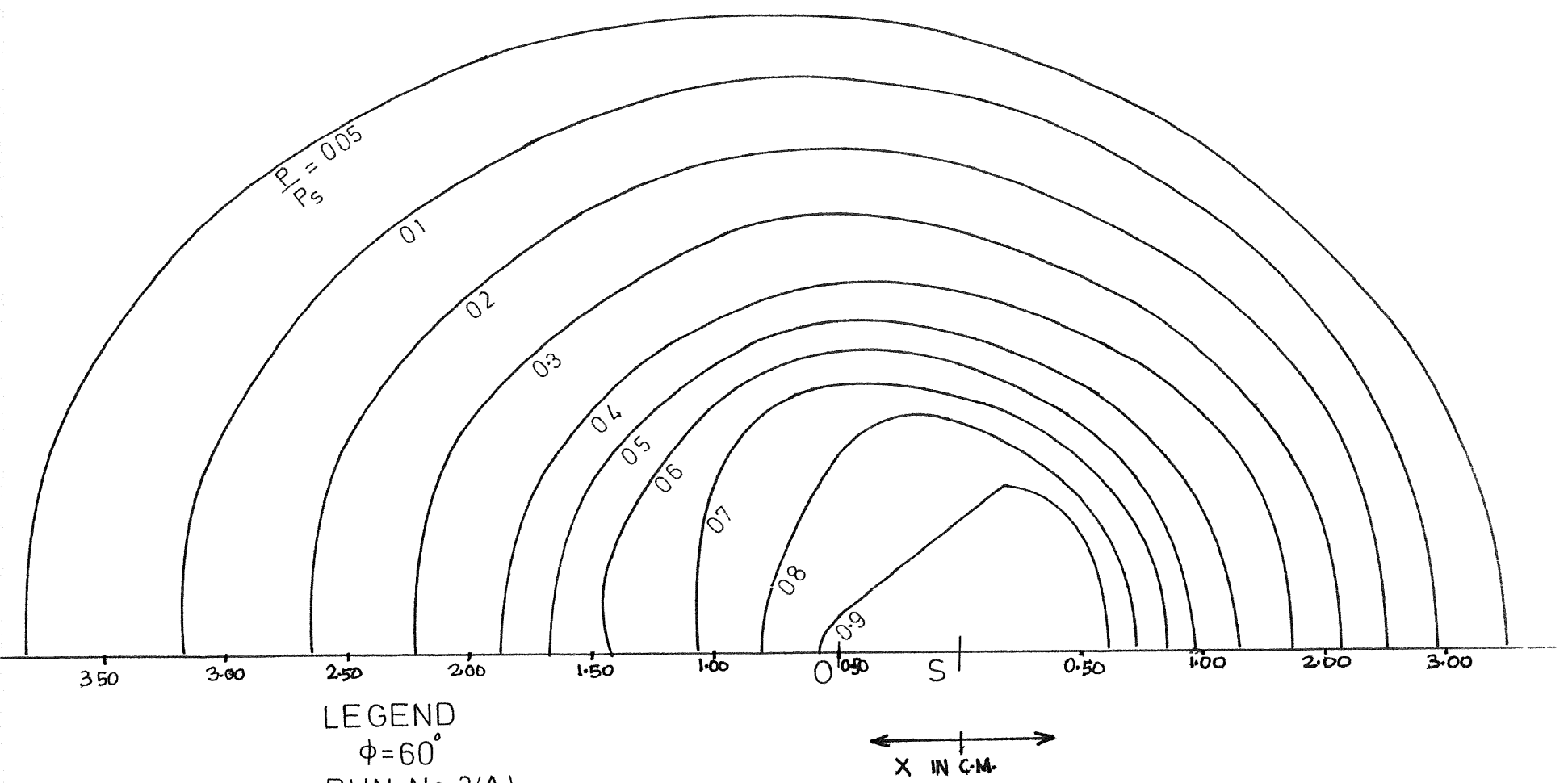

FIGURE 4 6 b PRESSURE CONTOURS

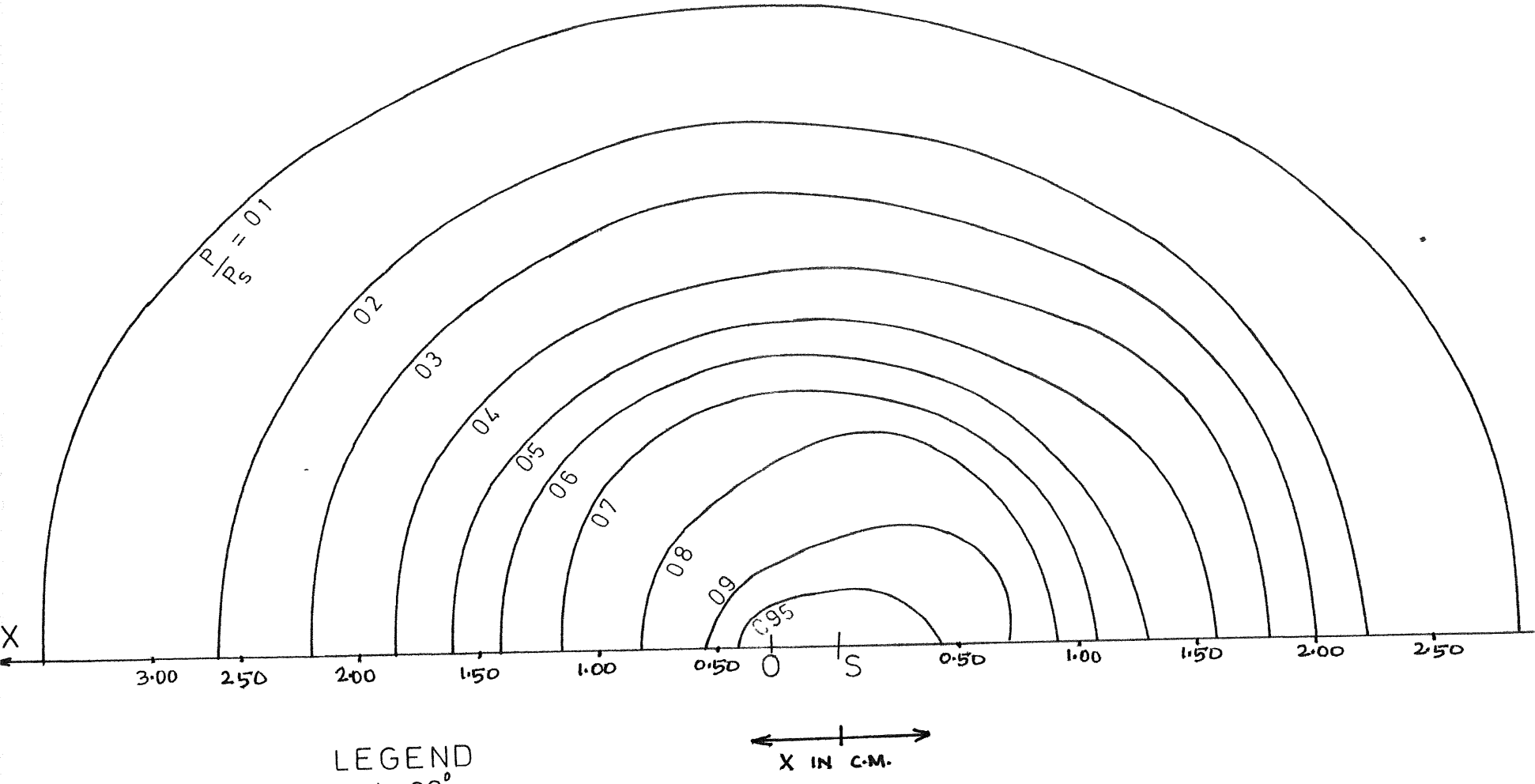

LEGEND
$\phi = 60^{\circ}$
RUN No 3(A)

FIGURE 46c PRESSURE CONTOURS

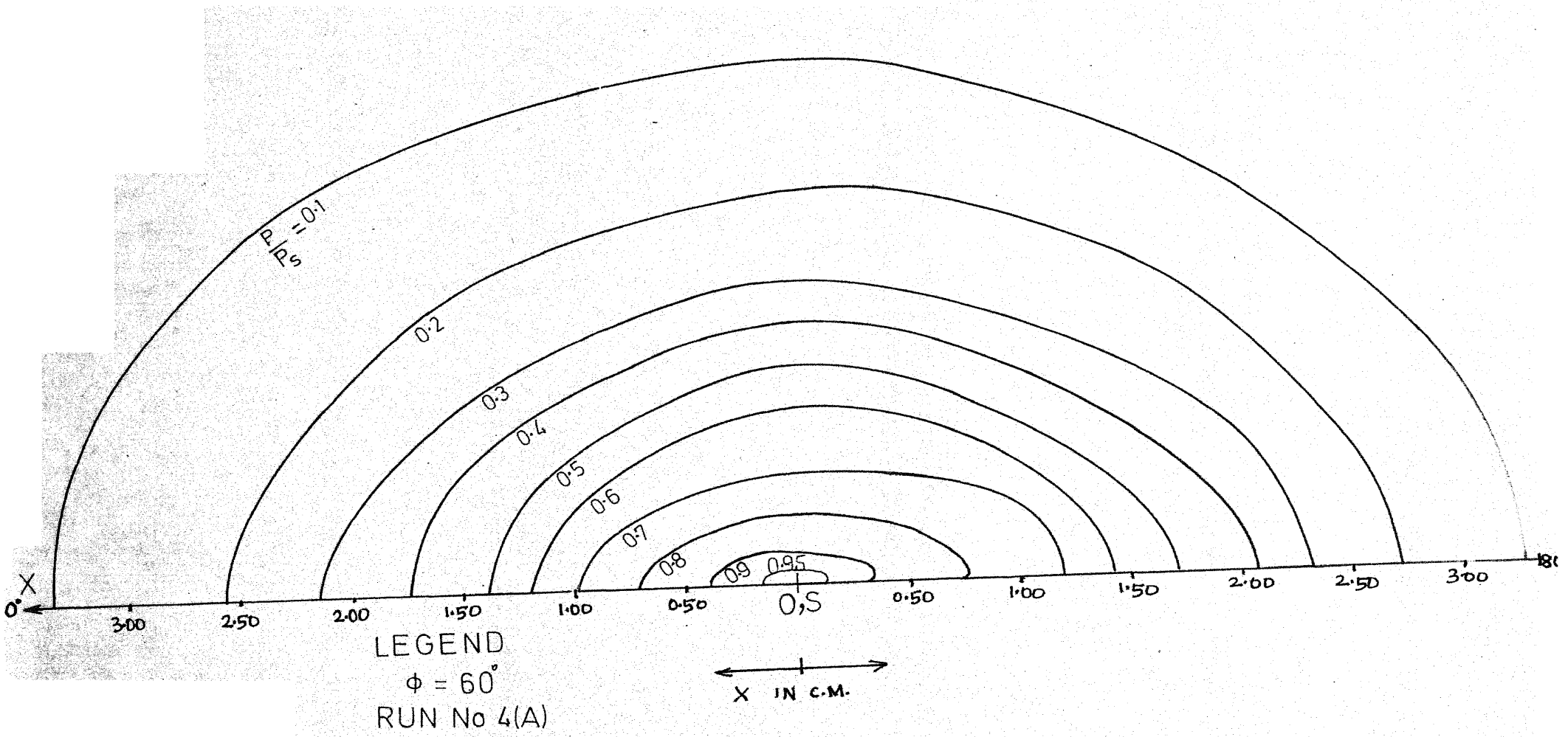

FIGURE 4·6 d PRESSURE CONTOURS

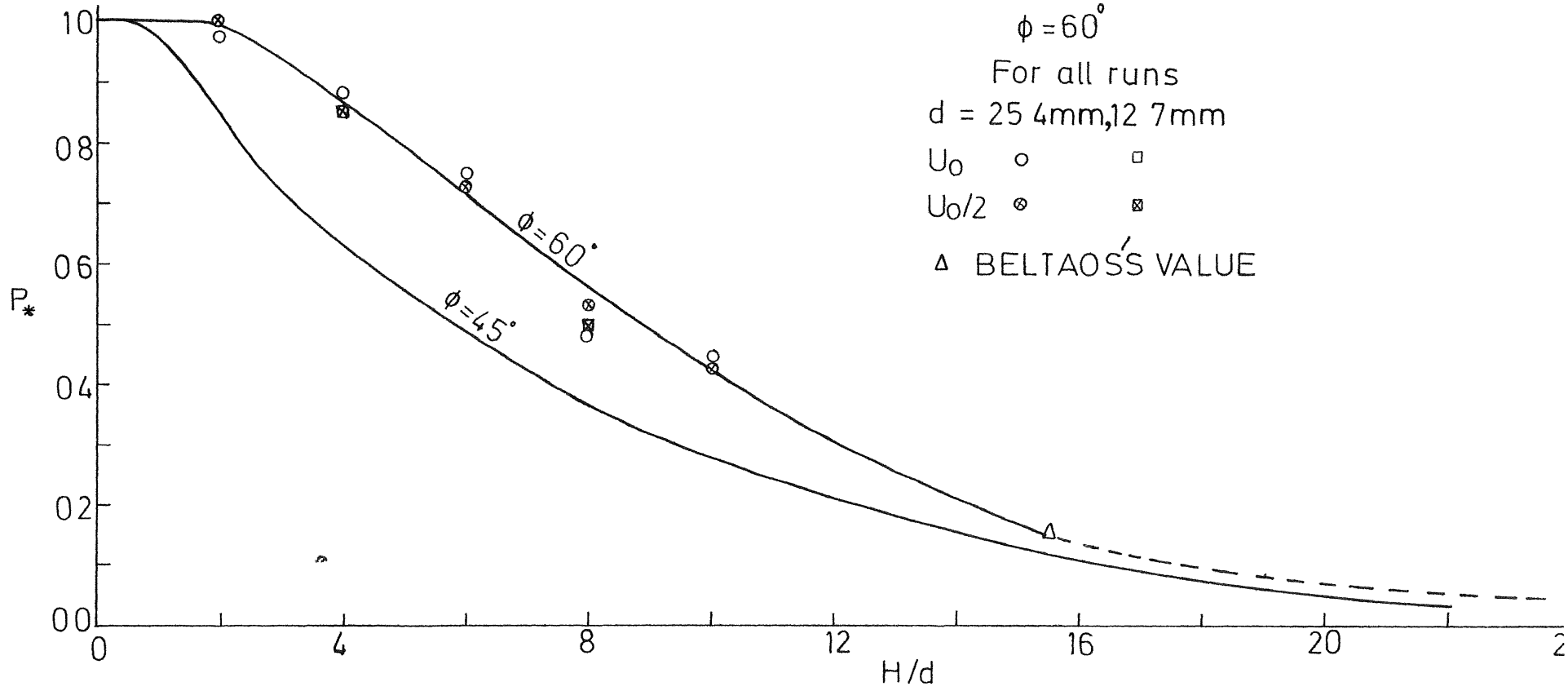

FIGURE 47 STAGNATION PRESSURE VARIATION

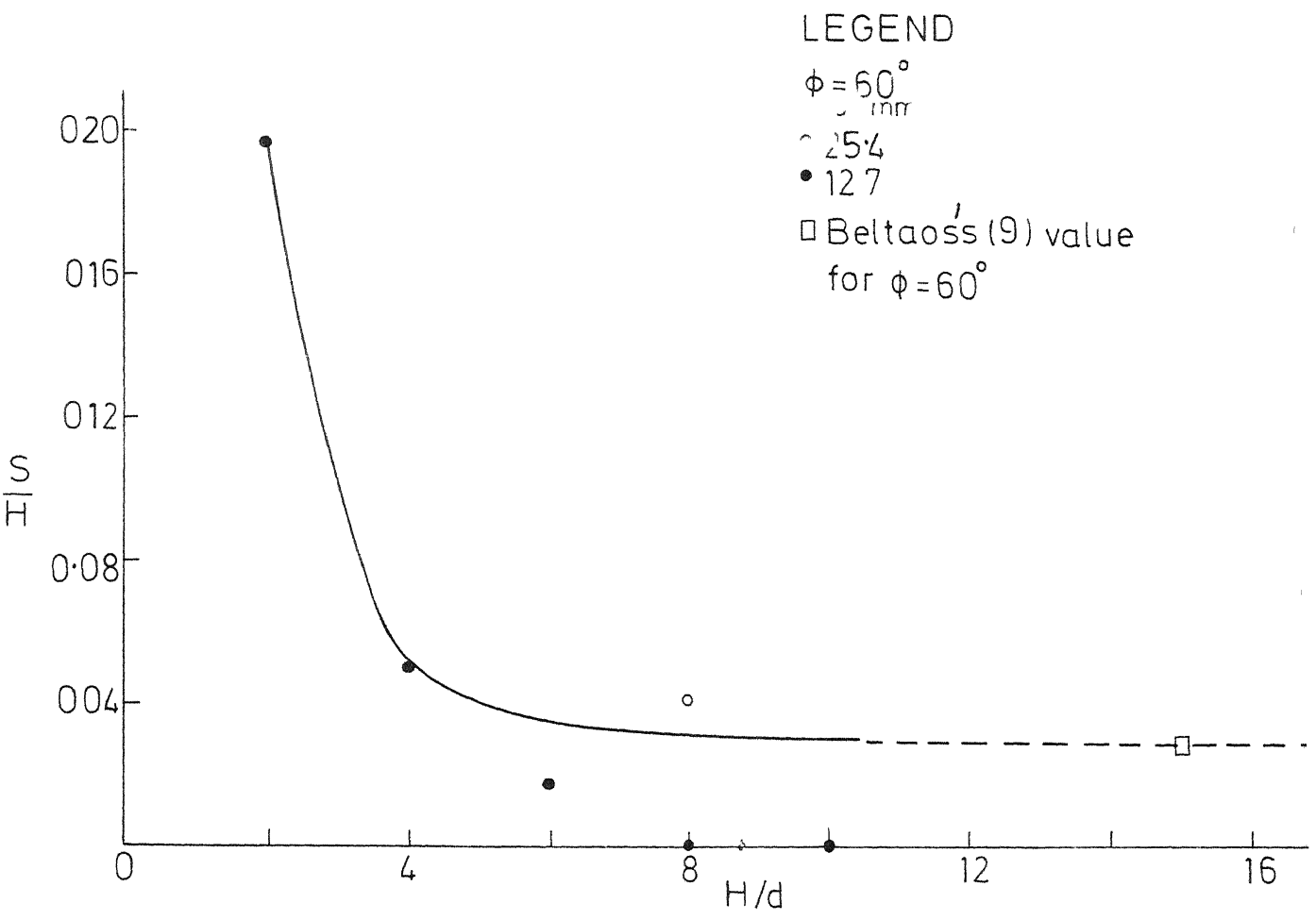

FIGURE 4·8 LOCATION OF STAGNATION POINT

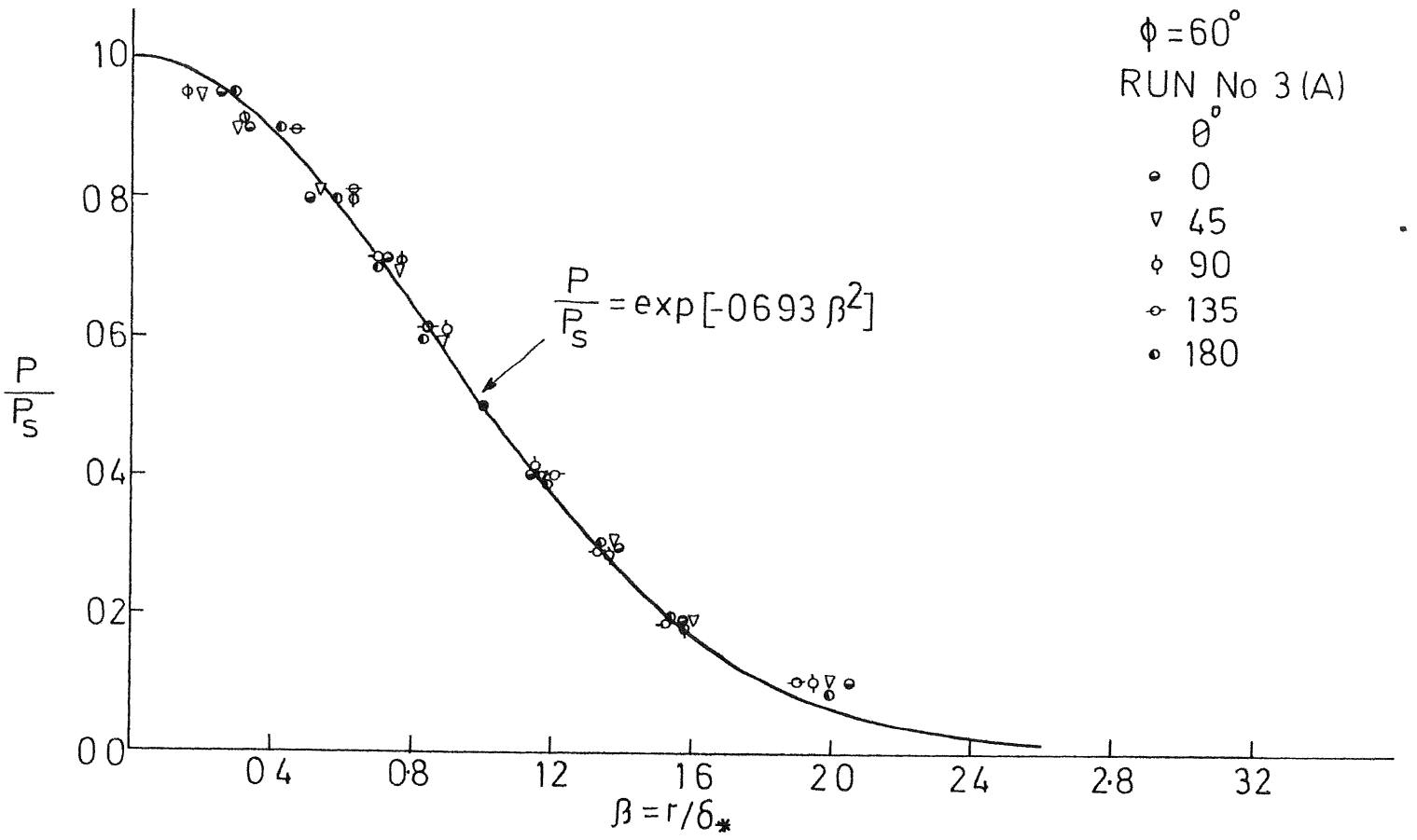

FIGURE 49a SIMILARITY OF PRESSURE PROFILE

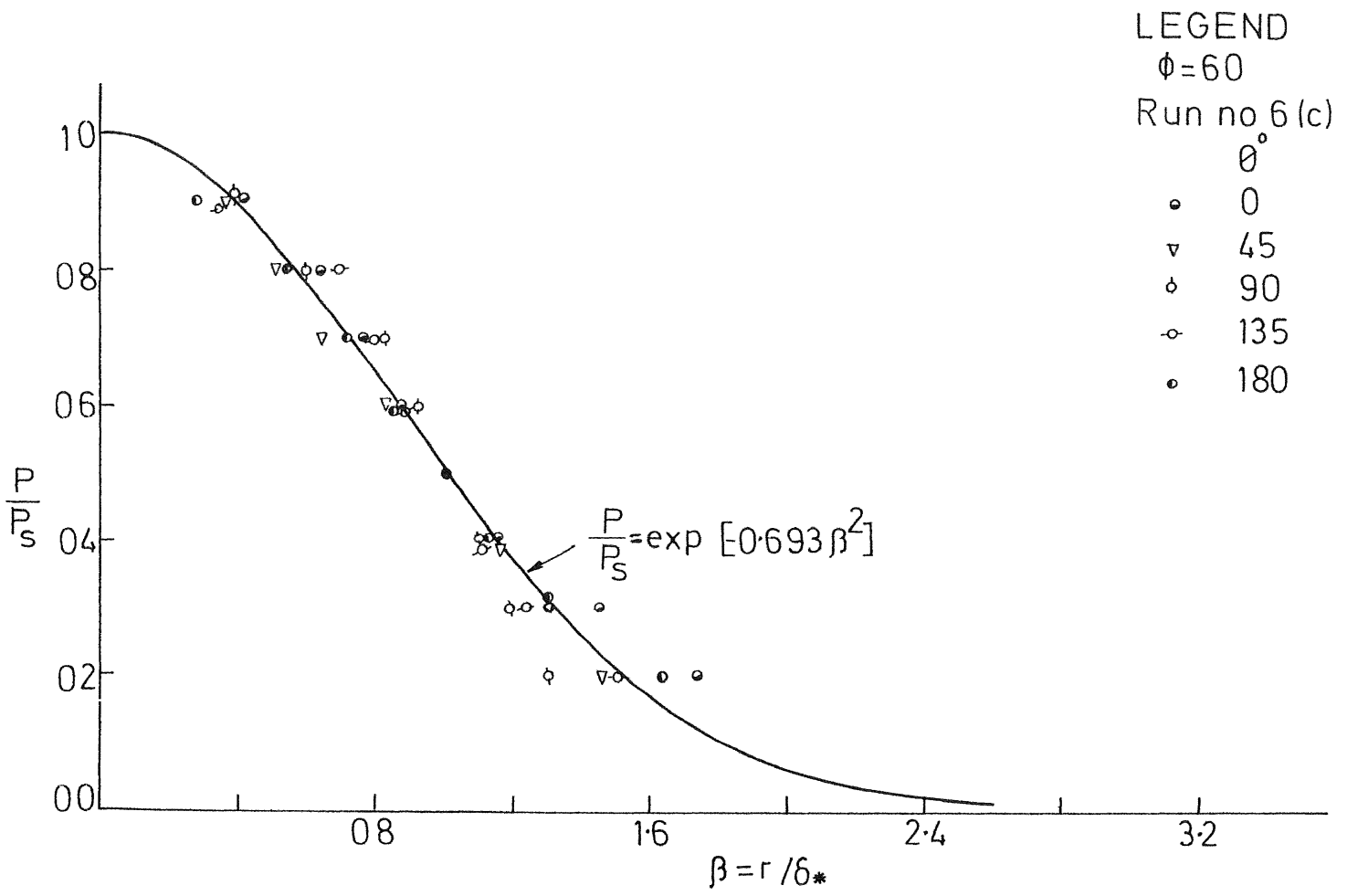

FIGURE 4.9b SIMILARITY OF PRESSURE PROFILE

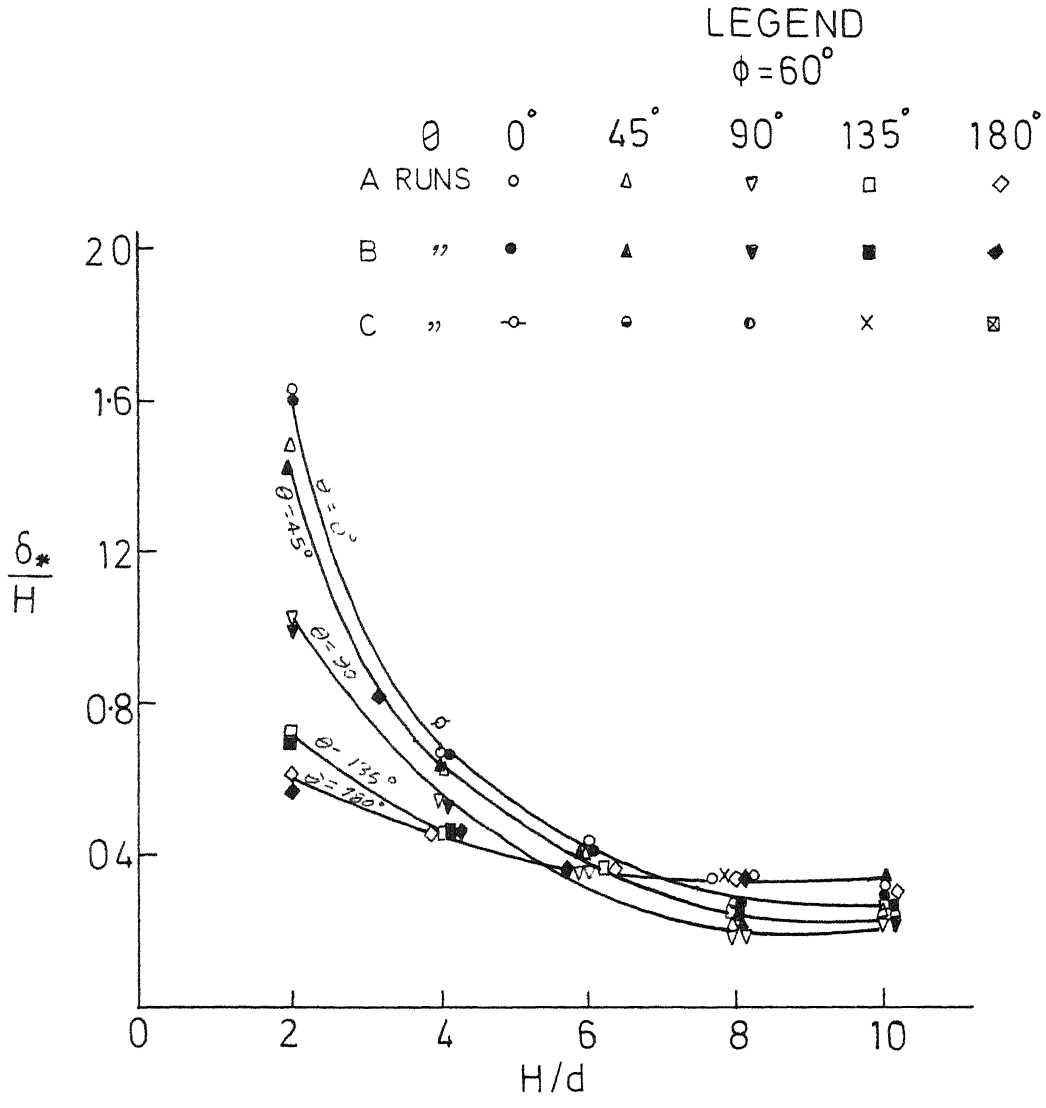

FIGURE 4.10 VARIATION OF LENGTH SCALE, δ_*

CHAPTER 5

CONCLUSIONS

The main objective of present study was to investigate further information on the behaviour of short jet oblique impingement. From the analysis and discussion of various results the following conclusions can be drawn:

1. In the wall jet region the velocity characteristics viz. the similarity plot and the length and velocity scales are not affected by the nature of impinging jet.

2. At $r \geq 3.0$ d, the wall jet is fully developed for all values of H/d. This could be taken as the safe value beyond which fully developed wall jet flow exits.

3. The pressure profile can be expressed by the Gaussian equation $\frac{P}{P_s} = \exp\left(-0.693\,\beta^2\right)$ which is independent of the nature of impingement.

4. The stagnation pressure, P_s and stagnation point, S are function of H/d. In these aspects the short jet impingement has a markedly different effect than the long jet impingement.

Thus it can be concluded that short jet impingement affects only some characteristics of the impingement region such as the location of stagnation point and stagnation pressure. However pressure similarity profile is not affected by it. Also the wall jet region characteristics are not at all affected.

APPENDIX A-1

REFERENCES

1. ABRAMOVICH, G.N., "The Theory of Turbulent Jets", Tech. Editing by L.H. Schindel, the M.I.T. Press, Massachussetts Institute of Technology, Cambridge, Massachussets, 1963.

2. BAKKE,P. , "An Experimental Investigation of a Wall Jet", J. of Fluid Mechanics, No.2, 1957, pp. 467-472.

3. BELTAOS, S., "Oblique Impingement of Circular Turbulent Jets", J. of Hydraulics Research, IAHR, Vol.14, No.1, 1976, pp. 17-36.

4. BELTAOS, S. and N. RAJARATNAM, "Circular Turbulent Impinging Jets", J. of Hyd. Div., Proc. ASCE, Vol.100, HY 10, October 1974, pp. 1313-1328.

5. GLAUERT, M.B., "The Wall Jet", J. of Fluid Mechanics, 1, 1956, p. 625.

6. KAMOI, A. and H. TANAKA, "Measurement of Wall Shear Stress, Wall Pressure and Fluctuations in the Stagnation Region Produced by Oblique Jet Impingement", Fluid Dynamics Measurements, Conference Papers, Vol.1, 1972, pp. 217-227.

7. NAIB, S.K.A., "Deflexion of a Submerged Round Jet to Increase Lateral Spreadings", La Houille Blanche, No.6, 1974.

8. PATEL, V.C., "Caliberation of the Preston Tube and Limitations on its Use in Pressure Gradients", J. of Fluid Mechanics, Vol.23, 1965, pp. 185-208.

9. PRESTON, J.H., "The Determination of Turbulent Skin Friction by Means of Pitot Tube", J. of Royal Aeronautical Society, London, England, Vol.58, Feb.1954, pp. 109-121.

10. RAJARATNAM, N., "Turbulent Jets", Elsevier Publishing Co., Amsterdam, The Netherlands.

11. SINHA, D.K., "Oblique Impingement of a Circular Jet", thesis submitted for Master of Technology degree at Indian Institute of Technology, Kanpur under the guidance of Dr. K. Subramanya.

APPENDIX A-2

EXPERIMENTAL DATA

Barometric pressure = 72 cm (Ave.) of mercury

Kinematic viscosity of air, $\nu_a = 1.5 \times 10^{-5}$ $m^2/sec.$ (at 30^oC)

Mass density of air, $\rho_a = 0.126$ kg/m^3 (at 20^oC)

Unit weight of air , $\gamma_a = 1.208$ kgf/m^3 (at 20^oC)

S.No.	Run No.	d in mm	H in mm	H/d	U_o in m/sec.	$\frac{U_o^2}{2}$ in kg/m^2	P_s in kg/m^2	$P_s/(\rho_a U_o^2/2)$	s in mm	s/H	Temperature t^o C
1	2	3	4	5	6	7	8	9	10	11	12
1	1(A)	25.4	50.8	2.0	52.0	150.1	147.0	0.980	10.00	0.197	35.0
2	1(B)	25.4	50.8	2.0	36.8	75.2	75.0	0.997	10.00	0.197	36.0
3	2(A)	25.4	101.6	4.0	52.0	150.1	132.0	0.880	5.00	0.050	35.5
4	2(B)	25.4	101.6	4.0	36.9	74.9	64.0	0.854	5.00	0.050	37.5
5	3(A)	25.4	152.4	6.0	55.7	173.7	130.0	0.748	2.75	0.018	31.5
6	3(B)	25.4	152.4	6.0	39.4	86.9	64.0	0.736	2.75	0.018	31.0
7	4(A)	25.4	203.2	8.0	51.8	150.3	75.0	0.500	0.00	0.000	33.0

Contd.....

Appendix A-2 contd..

1	2	3	4	5	6	7	8	9	10	11	12
8	4(B)	25.4	203.2	8.0	36.6	75.0	36.2	0.483	0.00	0.00	33.0
9	5(A)	25.4	254.0	10.0	52.0	150.1	67.0	0.446	0.00	0.00	36.0
10	5(B)	25.4	254.0	10.0	36.8	75.2	32.4	0.431	0.00	0.00	34.0
11	6(C)	12.7	101.6	8.0	51.8	150.3	80.0	0.532	4.40	0.043	31.0
12	6(D)	12.7	101.6	8.0	36.6	75.0	35.2	0.470	4.40	0.043	33.0
13	7(C)	12.7	50.8	4.0	52.0	150.1	128.0	0.853	0.00	0.00	35.0

APPENDIX A-3

A TYPICAL EXAMPLE

Problem:

Find the wall pressure and the velocity of flow at y = 1 cm, at the radial distances of 5 cm and 15 cm respectively from the Geometric centre (G.C.) of the circular plate along $\theta = 0°$. Also find the location of stagnation point.

The required details are given below:

Dia. of the nozzle, d = 2.54 cm

Length of impingement, H = 10.16 cm

Nozzle exit velocity, U_o = 52 m/sec.

Air temperature t°C = 35.5

Mass density of air at 35.5°C = 0.111 kg/m^3

Velocity scale, u_m variation as per the equation $\frac{U_o}{u_m} = m \frac{r}{d}$ and velocity length scale variation as per the equation $\delta = 0.076\, r$ where, r is the radial distance measured from stagnation point. Also plots of location of stagnation point, length scale, δ^*, stagnation pressure variation, similarity pressure profile and similarity radial velocity profile are given.

Solution:

Wall pressure calculation:

$$\frac{H}{d} = \frac{10.16}{2.54} = 4.0$$

From the plot of location of stagnation point

When $H/d = 4.0$ $\quad s/H = 0.05$

$$s = 0.05 \times 10.16 = 0.51 \text{ cm}$$

Stagnation point 'S' is located at 0.51 cm upstream of G.C.

Radial distance from the G.C. at which the pressure is required = 5.0 cm.

So from the stagnation point the distance, $r = 5 + 0.51$

$$= 5.51 \text{ cm.}$$

From the plot of length scale, δ_*

when $H/d = 4.0$ and $\theta = 0$, corresponding $\delta_*/H = 0.68$

$$\text{So} \quad \delta_* = 0.68 \times 4.0 \times 2.54$$

$$= 6.9 \text{ cm.}$$

$$\text{Therefore,} \quad \frac{r}{\delta_*} = \beta = \frac{5.51}{6.9} = 0.80$$

Looking at the similarity pressure profile the above r/δ_* value is well inside the impingement region.

From the stagnation pressure variation plot for $H/d = 4.0$ the corresponding $P_* = \dfrac{P_s}{(\rho U_o^2/2)} = 0.865$

$$P_s = 0.865 \times \frac{\rho_a U_o^2}{2}$$

$$= 0.865 \times 0.111 \times \frac{52^2}{2} = 130 \text{ kg/m}^2$$

Using the semi-empirical equation

$$\frac{P}{P_s} = \exp (- 0.693\beta^2)$$

$$P = P_s \exp (- 0.693\beta^2)$$

$$= 130 \exp (-0.693 \times 0.8^2)$$

$$= 83 \text{ kg/m}^2$$

Wall pressure at the radial distance of 5 cm. from G.C. is 83 kg/m^2

Velocity calculation:

$$5d = 5 \times 2.54 = 12.70$$

Radial distance at which velocity is required, from the stagnation point, r = 15.51 cm. > 5 d.

So this section is in the fully developed wall jet region.

Using the equation $\frac{U_o}{u_m} = m \frac{r}{d}$

m for $\theta = 0$ is 0.416

$$u_m = \frac{U_o d}{m r} = \frac{52 \times 2.54}{0.46 \times 15.51} = 18.5 \text{ m/sec.}$$

From the equation $\delta = 0.076 \times r$

$$\delta \text{ at } r = 15.51 \text{ cm. is } = 0.076 \times 15.51$$

$$= 1.18 \text{ cm.}$$

$$\text{at } y = 1 \text{ cm.} \quad \frac{y}{\delta} = \frac{1.0}{1.18} = 0.85$$

From the similarity of radial velocity profile

$$\text{at } y/\delta = 0.85 \quad u/u_m = 0.61$$

$$u = 0.61 \times 18.5$$

$$= 11.3 \text{ m/sec.}$$

So the radial velocity at $y = 1.0$ cm. from the plate level at the radial distance of 15.0 cm. from G.C. = 11.3 m/sec.

PART B

OBLIQUE IMPINGEMENT OF FREE FLOW JET (Water jet in Air)

CHAPTER 6

EXPERIMENTAL STUDY

6.1 Literature Review:

Normal impingement of circular water jet on plane surface has been experimentally and analytically studied for the formation of hydraulic jump by Koloseus and Ahmad (2) and by Arbhabirama and Wan (1). The case of oblique impinging jets is complicated due to the non-axisymmetry characteristics of flow over the plane surface after impingement. Literature available on the study of oblique impinging free flow jet is practically nil, except one exploratory study by Yao (3) for the hydraulic jump formation after impingement. However, Yao (3) proceeded his study on the assumption that the velocity of flow in the radial flow region surrounded by hydraulic jump, which he calls as the depressed area, is same as that of the nozzle exit velocity which is erroneous as it is not practically feasible for a spreading flow.

Since there were no useful available literature on this topic, this study was essentially of an exploratory nature to get basic parameters affecting the flow and to

study the nature of the flow qualitatively and quantitatively.

6.2 Experimental Investigation:

The purpose of the experiments was to study the characteristics of free flow jet impingement on plane surface with length of impingement H = 1d and impingement angle, $\phi = 60°$. Water was used as the jet medium and it travelled through air before impingement. Two nozzles of internal exit diameters d = 38.1 mm and 50.0 mm were used. The cylindrical system (r, θ , y) with the origin at the stagnation point, S is used to describe the different flow regions. (See Figure 1.2). A total number of 4 experiments were conducted and their particulars are summarized in Table 1.

TABLE 1.

DETAILS OF EXPERIMENTS

Angle of impingement, $\phi = 60°$
Temperature (mean) t° C = 30°
Kinematic viscosity of water $\nu_w = 0.804 \times 10^{-6} m^2/sec$ (at 30°C)

S.No.	Run No.	Discharge, Q in $cm^3/sec.$	Nozzle dia. d mm	H/d	Nozzle exit velocity, U_o m/sec.	Reynolds No. $R_o = U_o d/\nu_w$
1	1	8840.0	50.0	1.0	4.50	2.80×10^5
2	2	10640.0	50.0	1.0	5.42	3.37×10^5
3	3	9230.0	38.1	1.0	8.10	3.84×10^5
4	4	10640.0	38.1	1.0	9.35	4.42×10^5

6.3 Experimental Set-up:

Figure 6.1 shows the schematic diagram of the experimental set-up used for the study. A table was made with angle irons over which a circular tank of dia.182.4 (6') made from 1.6 mm (1/16") thick steel plates was placed. A 10 H.P. pump with control outlet valve delivered water from the storage tank through a reinforced hose-pipe of dia. 63.5 mm (2.5") and through a G.I. pipe of dia. 63.5 mm (2.5") with nozzle connected at its end. The G.I. pipe was slant at $\phi = 60°$ and it was kept in position by the clamp as shown in Figure 6.1. The jet would strike a 6.35 mm (1/4") thick by 152.4 cm (5') dia. circular smooth surface aluminium plate placed inside the tank. The level of the plate was adjusted by means of screws. The jet centre line coincided with the geometric centre of the plate. Markings made at 1 cm interval were used for measurement purposes along radial lines divided at $\theta = 30°$. Along $\theta = 0°$ and $\theta = 30°$ radial lines, suitably spaced static pressure taps of 1.6 mm dia. were present for a distance of about 10 cm in each radial line from the geometric centre, C. A 15 cm (6") dia . G.I. pipe with control valve drains the water from the tank through the centre of the tank bottom. The drained water was let into a channel with a already calibrated V-notch at its end. Figure 6.2

shows the different views of the experimental set-up.

6.4 Measurements:

6.4.1 Pressure and velocity measurements:

Radial wall pressures were measured using vertical manometers. Two different sets of water manometer with 100 cm and 60 cm length tubes and one vertical mercury manometer (maximum pressure 24.7 kg/cm^2) were used. Radial velocity was measured using total head tube which had a hypodermic tube of size 1.60 mm O.D. and 1.25 mm I.D. and which was connected to a gauge with vernier arrangement of least count 0.1 mm. The gauge was brought to any required position over the plate by moving the carrier, which carries the gauge, on the rail.

6.4.2 Depth measurement:

Conventional method of measuring the water depth using point gauge was found not suitable due to the inability in determining whether the pointer just touches the water surface. This difficulty was due to high velocity of flow with moderately less depth. To overcome this difficulty an electronic water sensor was fabricated. The details of which are given in Appendix B-2. The indicator lamp in

the circuit glows as soon as the gauge pointer touches the water surface. Thus the water surface level was noted and the datum level was noted by lowering the gauge pointer until it touches the plate. The direct contact between the carrier and the rail on which the carrier moves was avoided by insulating the contacting portion with perspex sheet.

6.5 A Typical Experiment:

The nozzle was fixed at an angle of $\phi = 60°$ and at the fixed length of impingement H = 1d measured along the jet centre line. Then the pump was started and the velocity, U_o at the nozzle exit was adjusted by controlling the pump valve.

The pressure taps were connected to the vertical manometers available depending upon the range of pressures. Pressure measurements along $\theta = 0°$ and $\theta = 30°$ radial lines were done till the pressure corresponding to the depth of water value reached in each radial direction.

The velocity observations were recorded with total head tube and the total head was measured on a vertical mercury manometer. Along each radial line, except at $\theta = 180°$ where measurement was not possible, velocity was measured at 12 sections each at 5 cm apart and at each section radial

velocity components were measured at number of points depending upon the variation of the velocity and depth of flow in that section. However the number of sections for velocity measurements were restricted in some radial lines due to depth of flow being of the order of the diameter of the total head tube.

The depth was measured at each section wherever the velocity measurement was made. The water surface level was noted as soon as the indicator lamp of the Electronic water sensor glows when the pointer touches the water surface. The datum at the same section was also measured.

The level of water in the sump well of the channel was noted for finding the discharge through the V-notch.

Thus at about 220 sections velocity and depth measurements were made in all 4 runs. All the data collected are presented in Appendix B-3.

All the measurements were conducted at co-ordinate positions determined with reference to the geometrical centre of the plate due to its easy location. However, for analysis purposes they were converted to the co-ordinates with stagnation point, S as the origin. The error involved in this is believed to be negligible because the location of stagnation point was not very much removed from the geometrical centre, O in all the runs.

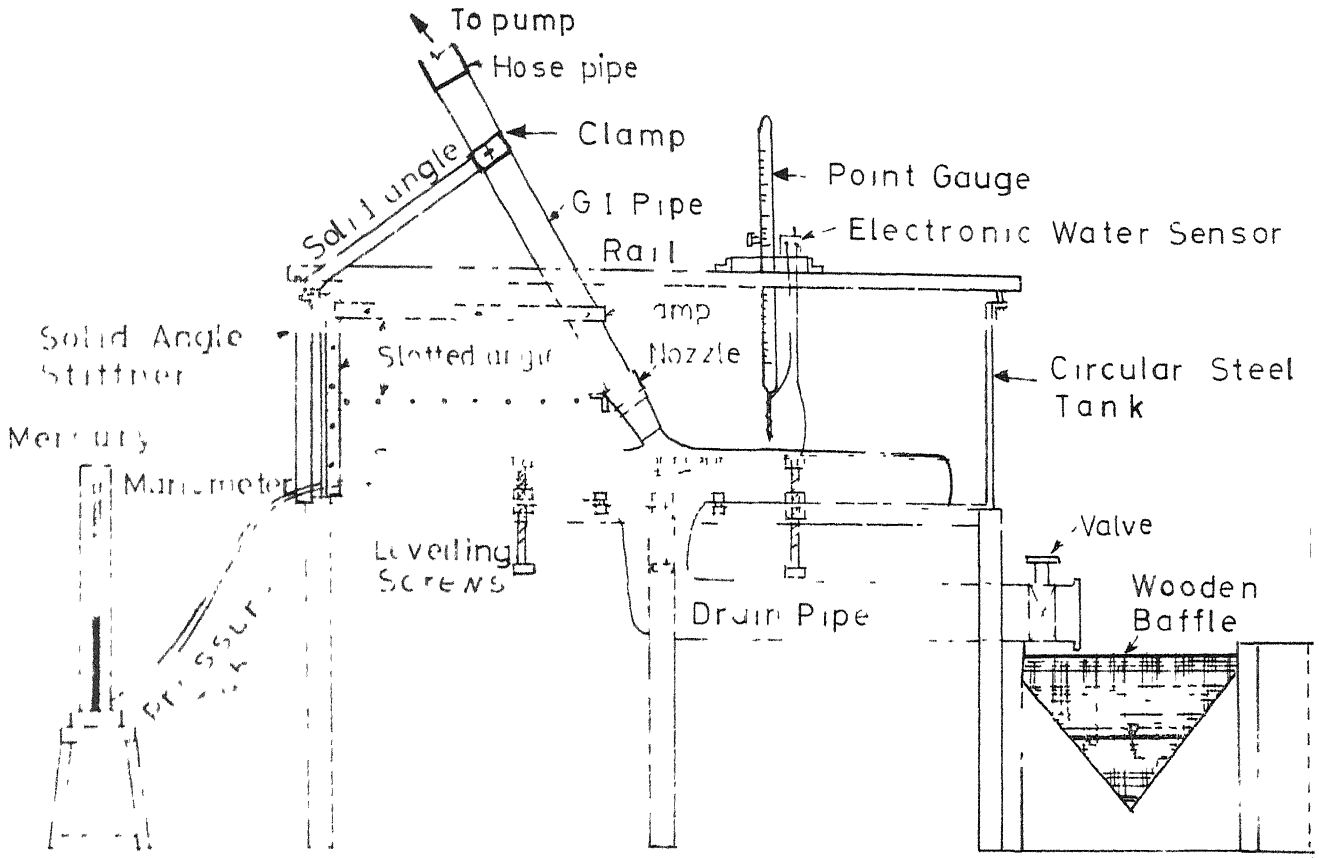

SECTIONAL ELEVATION

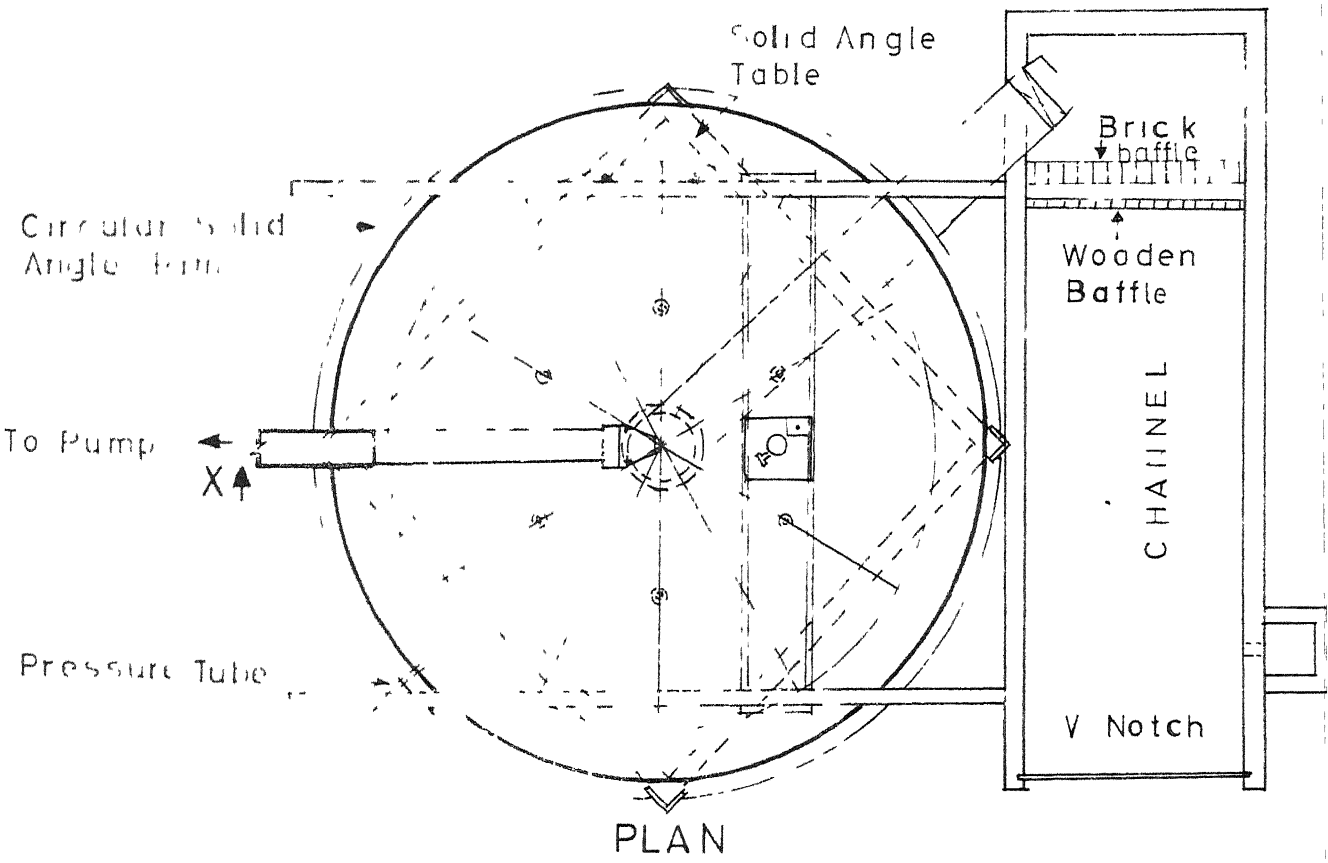

PLAN

FIGURE 6·1 SCHEMATIC DIAGRAM OF SET-UP

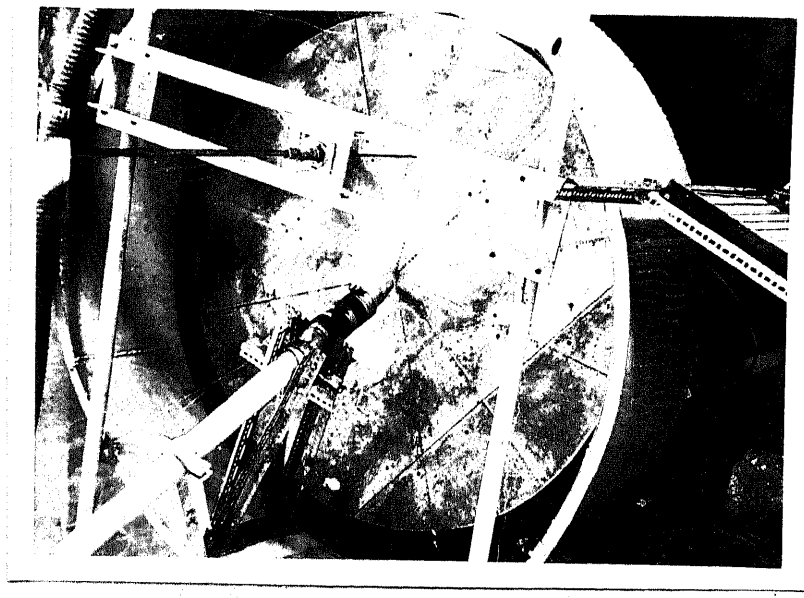

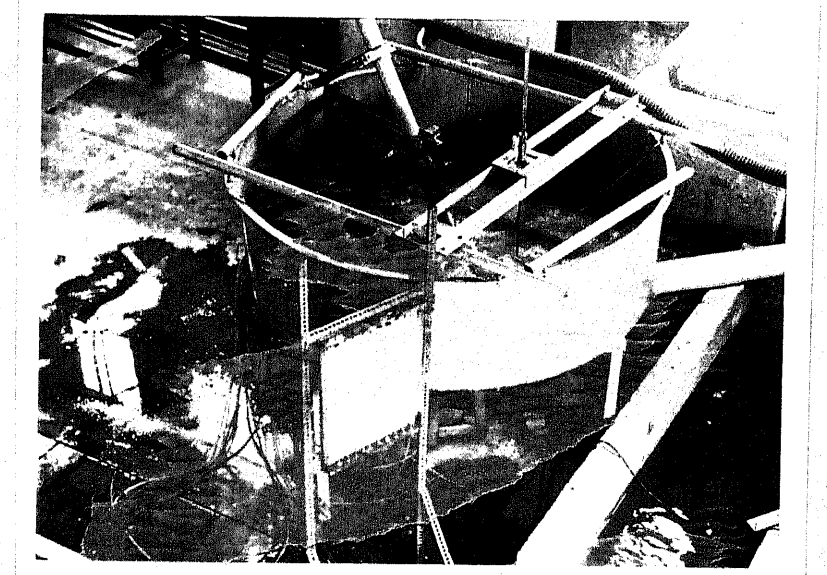

FIGURE 6.2 DIFFERENT VIEWS OF THE EXPERIMENTAL SET-UP

CHAPTER 7

ANALYSIS AND DISCUSSION

The data collected in the investigation were analysed to study the characteristics of impingement and radial flow regions and the discharge variation.

7.1 Impingement Region Investigation:

7.1.1 Location of stagnation point:

As the length of impingement is very small the stagnation pressure can be taken as $P_s = \frac{\rho_w U_o^2}{2}$; where ρ_w = mass density of water at experimental temperature t°C in kg/m^3.

The ratio of wall pressure to stagnation pressure was calculated for all the available wall pressure readings along $\theta = 0°$ and $\theta = 30°$ radial lines. The stagnation point was located by projecting the curve obtained between P/P_s and the radial distance from the geometric centre, O, until the curve touched the value of $\frac{P}{P_s} = 1.0$. It is found for both nozzles and for H/d = 1 the location of stagnation point is at s = 0.4 d upstream of O along $\theta = 0°$-$180°$ line.

7.1.2 Similarity of pressure profile:

After locating the stagnation point, a non-dimensional pressure profile is plotted for all runs to know the behaviour of pressure distribution in radial direction. (See Fig. 7.1). This plot is between P/P_s and r/δ_* where δ_* is the value of r measured from the stagnation point at $\frac{P}{P_s}=0.5$. This plot shows that P/P_s is independent of θ and U_o for a given ϕ and H/d. The obtained curve B is of Gaussian function type and can be expressed as

$$\frac{P}{P_s} = \exp(-0.693\ \beta^2), \text{ where } \beta = \frac{r}{\delta_*} .$$

This well agrees with the similar results obtained for short and long submerged jet impingement.

The length scale δ_* was found to be a function of H/d and θ for the given ϕ. The values of δ_*/H with $\theta = 0°$ and 30° were found to be 0.830 and 0.860 respectively for d = 50 mm and they were 1.050 and 1.100 respectively for d = 38.1 mm and they differ with the corresponding values of short submerged jet impingement. The reason may be attributed to the entrainment characteristics of the latter.

7.2 Radial Flow Region Investigation:

7.2.1 Mean velocity distribution:

Mean velocity of flow at any section is calculated by averaging the available radial component velocities at the section. A plot, as shown in Figure 7.2 a, between the calculated mean velocities along different radial lines and the corresponding radial distances was made and mean curves were obtained. These mean curves were used to plot equal velocity contours as shown in Figures 7.3a, 7.3b, 7.3c and 7.3d. It is seen that the curves deviate from the circular pattern of normal impingement as non-axisymmetry of flow exits on the plane surface.

7.2.2 Similarity of velocity profiles:

A non-dimensional velocity profile was plotted for each run in order to know the behaviour of mean velocity distribution in the radial direction. (See Figures 7.4a, 7.4b, 7.4c and 7.4d). The plot is between $\frac{u}{U_o}$ and $\frac{r}{r_*}$, where u = mean radial velocity at any section in m/sec and r_* = the value of r at $\frac{u}{U_o} = 0.5$. This was done only for the region beyond the impingement region.

It is seen from the above plots for all the runs the same curve C is obtained. This plot is found to be

independent of θ , and U_o. The obtained curve C is of Gaussian function type and can be expressed as

$$\frac{u}{U_o} = \exp\ (-0.693\ \alpha^2), \text{ where } \alpha = \frac{r}{r_*}$$

So it is found the mean velocity is distributed in the same manner as the wall pressure distributed along the radial direction.

7.2.3 Variation of length scale, r_*:

The length scale r_* i.e. the value of r at $\frac{u}{U_o} = 0.5$ is a function of θ as shown in Figure 7.5. It is seen that $\frac{r_*}{d}$ is independent of U_o for a given angle of impingement $\emptyset$ and H/d.

7.3 Discharge Variation:

Discharge within a circular sector of radius r and included angle d θ was calculated as follows:

Discharge, q = r x $\frac{d\theta \times \pi}{180^\circ}$ x Average depth at the subtending arc length x Average of mean velocity.

Many number of similar sectors were considered and the corresponding discharges were found, for the same radius, r.

Then all these segmental discharges were added up to get the cumulative discharges $\sum^{\theta} q$ or the discharge in any range of θ from $\theta=0°$. The discharge from $\theta=0°$ to $\theta=180°$ is denoted as $\sum^{\theta=180^{o}} q$. The same procedure is repeated for another radius r for the same run in order to have a check on the discharge calculation.

A plot is shown in Figure 7.6 between $\frac{\sum^{\theta} q}{\sum^{\theta=180^{o}} q}$ and θ in degrees. This plot shows the variation of discharge along the circumferential direction. Discharge variation for an axisymmetrical flow along the circumferential direction is also shown in Figure 7.6.

Figure 7.7 shows the variation of $\frac{q}{\sum^{\theta=180^{o}} q}$, where q is the discharge in the $d\theta$ segment, along θ. It is seen that $\frac{q}{\sum^{\theta=180^{o}} q}$ is independent of U_o and d.

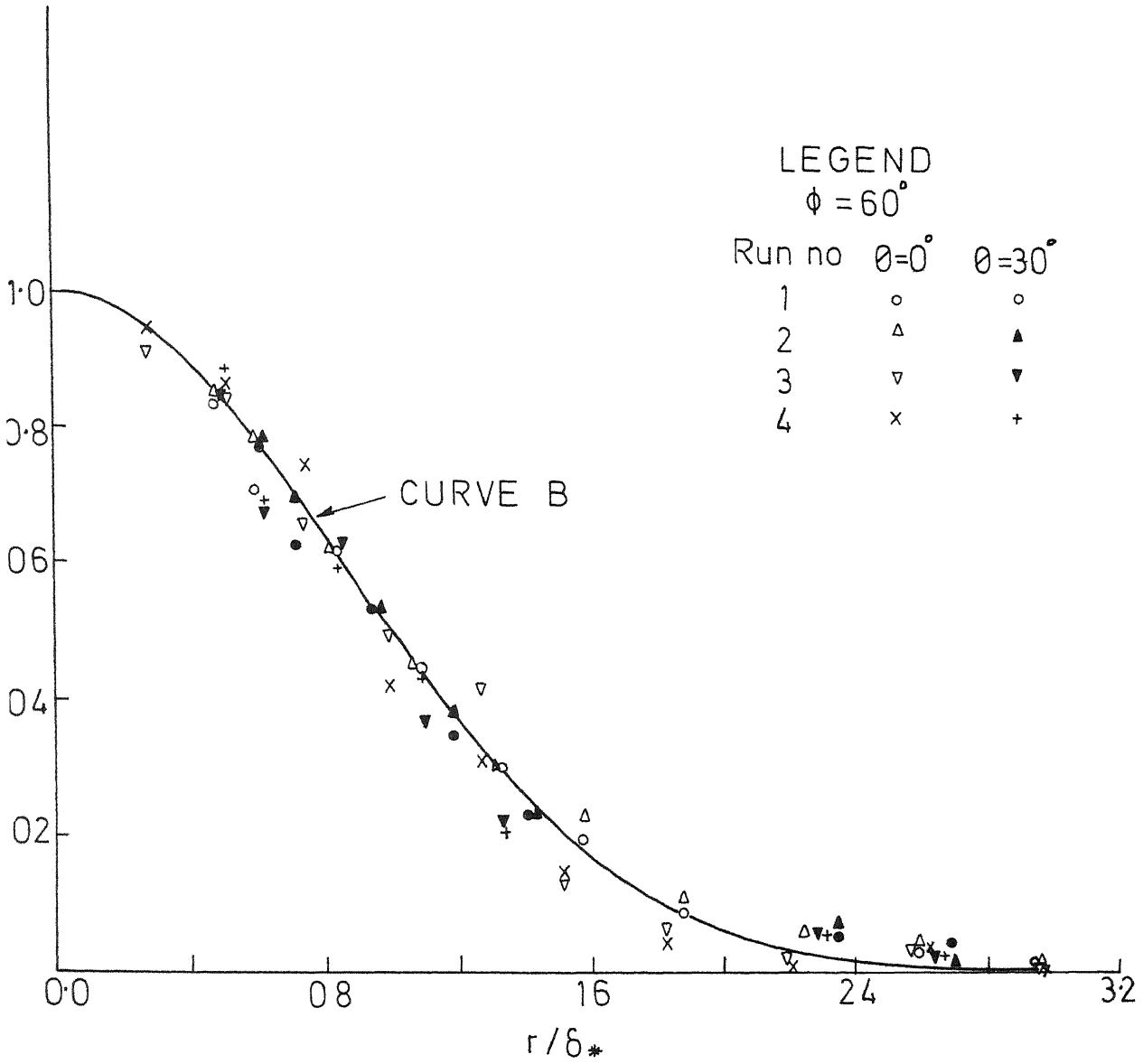

FIGURE 7·1 SIMILARITY PRESSURE PROFILE

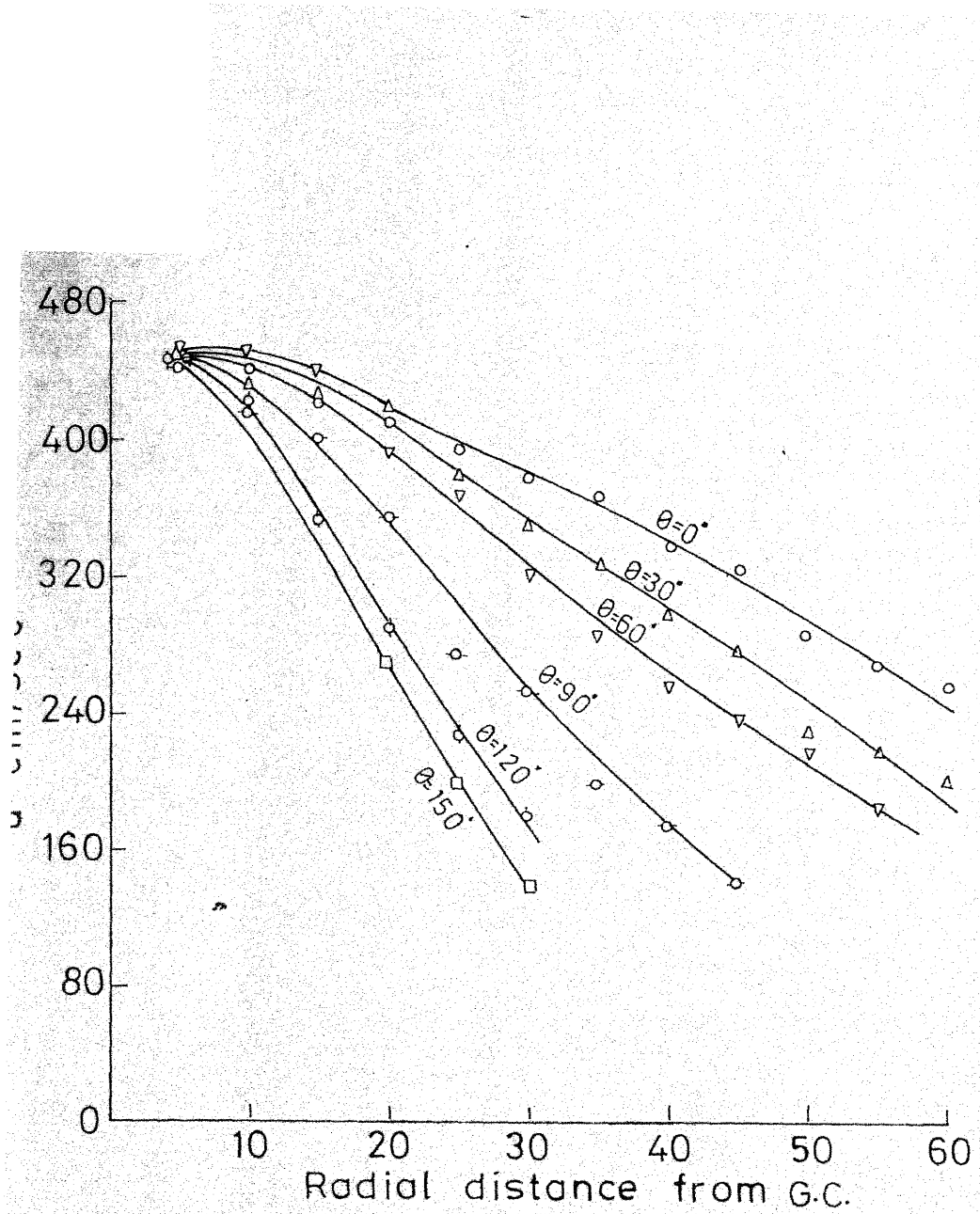

FIGURE 7·2a VELOCITY VARIATION

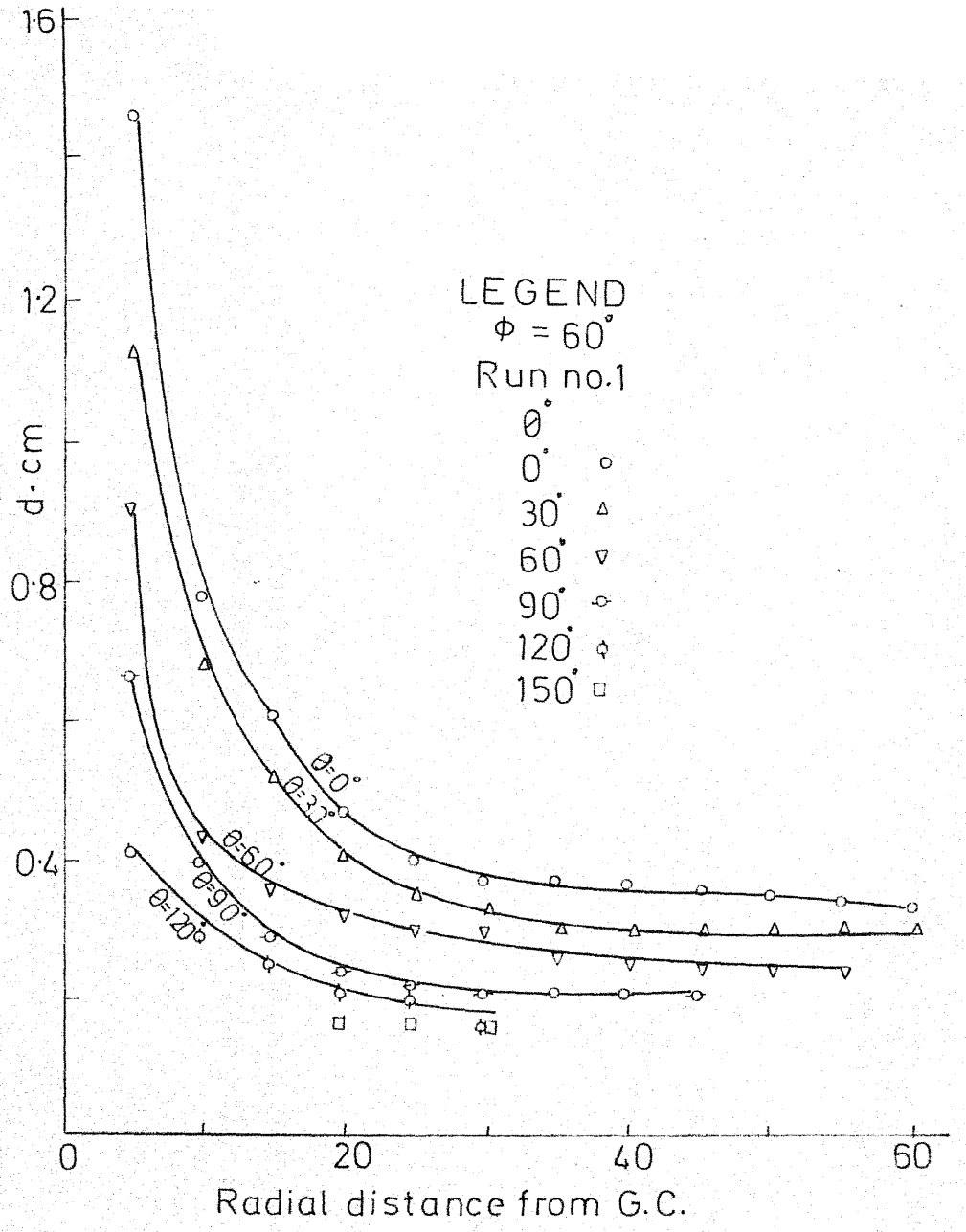

FIGURE 7·2 b DEPTH VARIATION

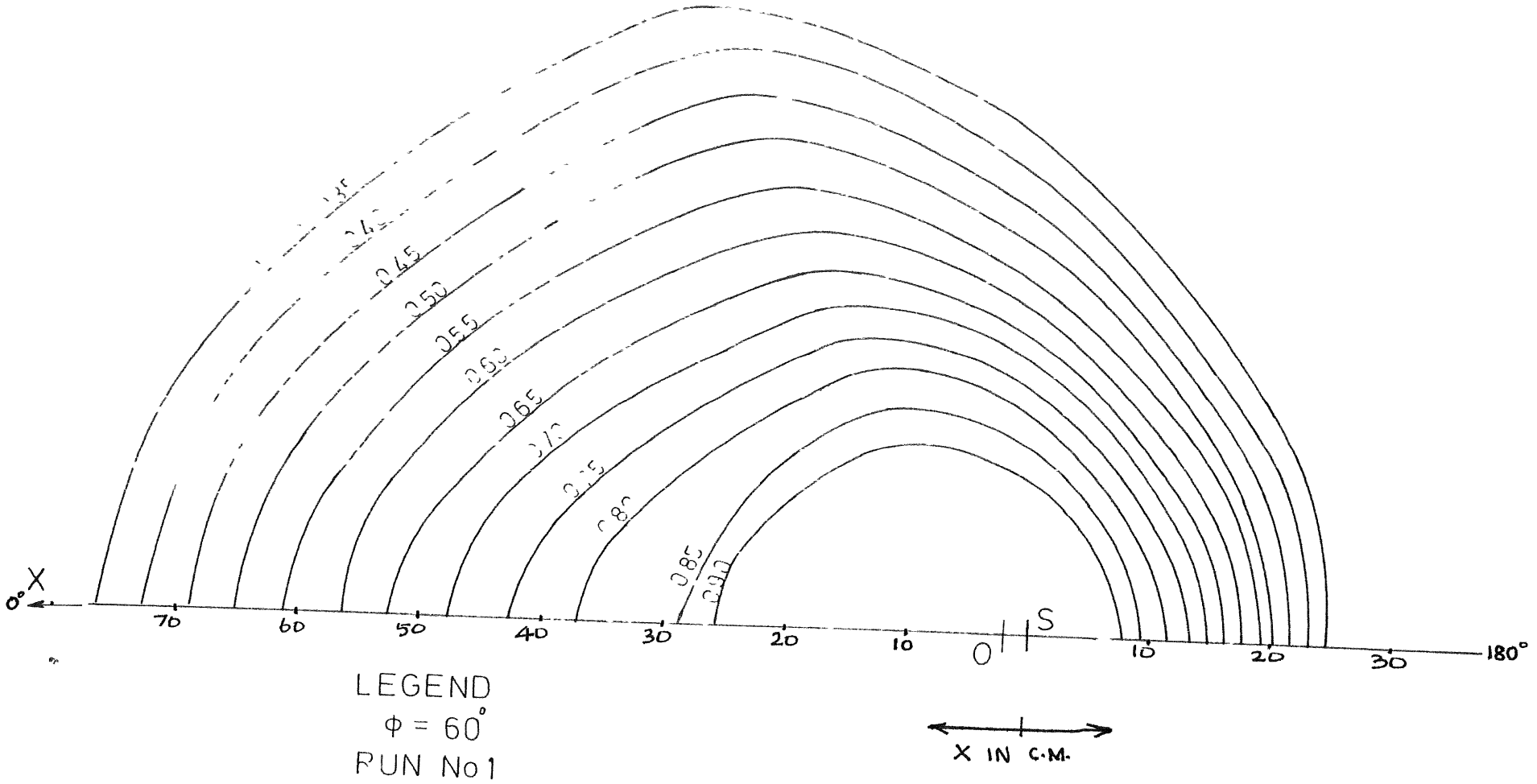

FIGURE 7·3 a MEAN VELOCITY CONTOURS

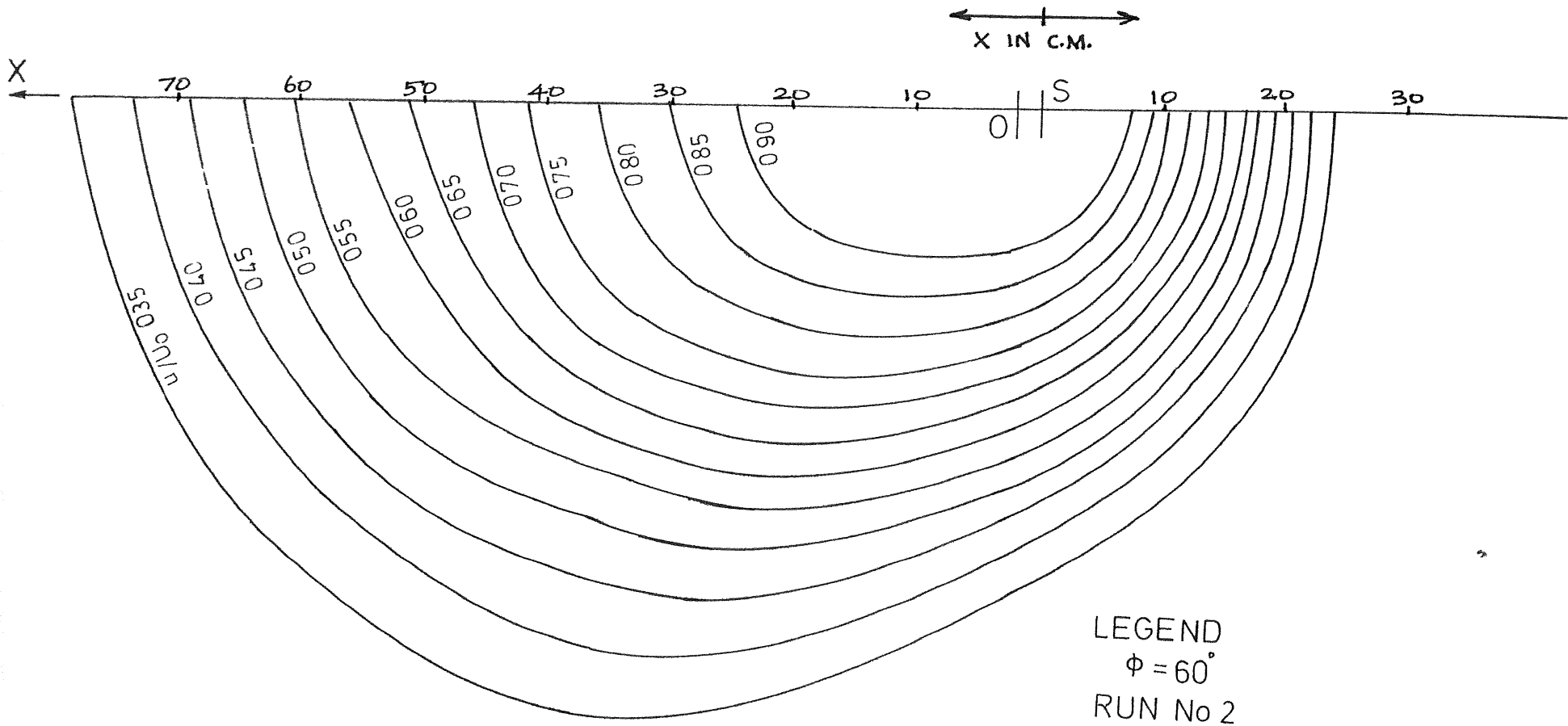

FIGURE 73 b MEAN VELOCITY CONTOURS

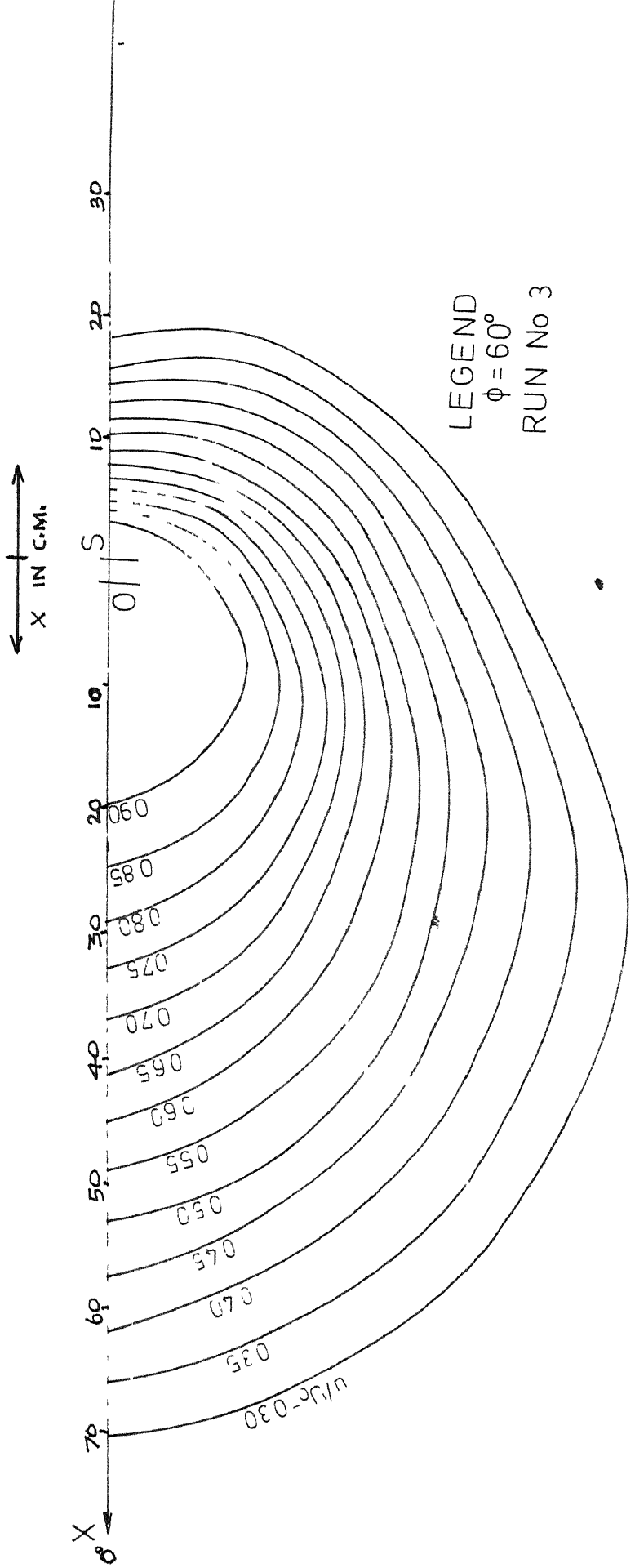

FIGURE 7.3 c MEAN VELOCITY CONTOURS

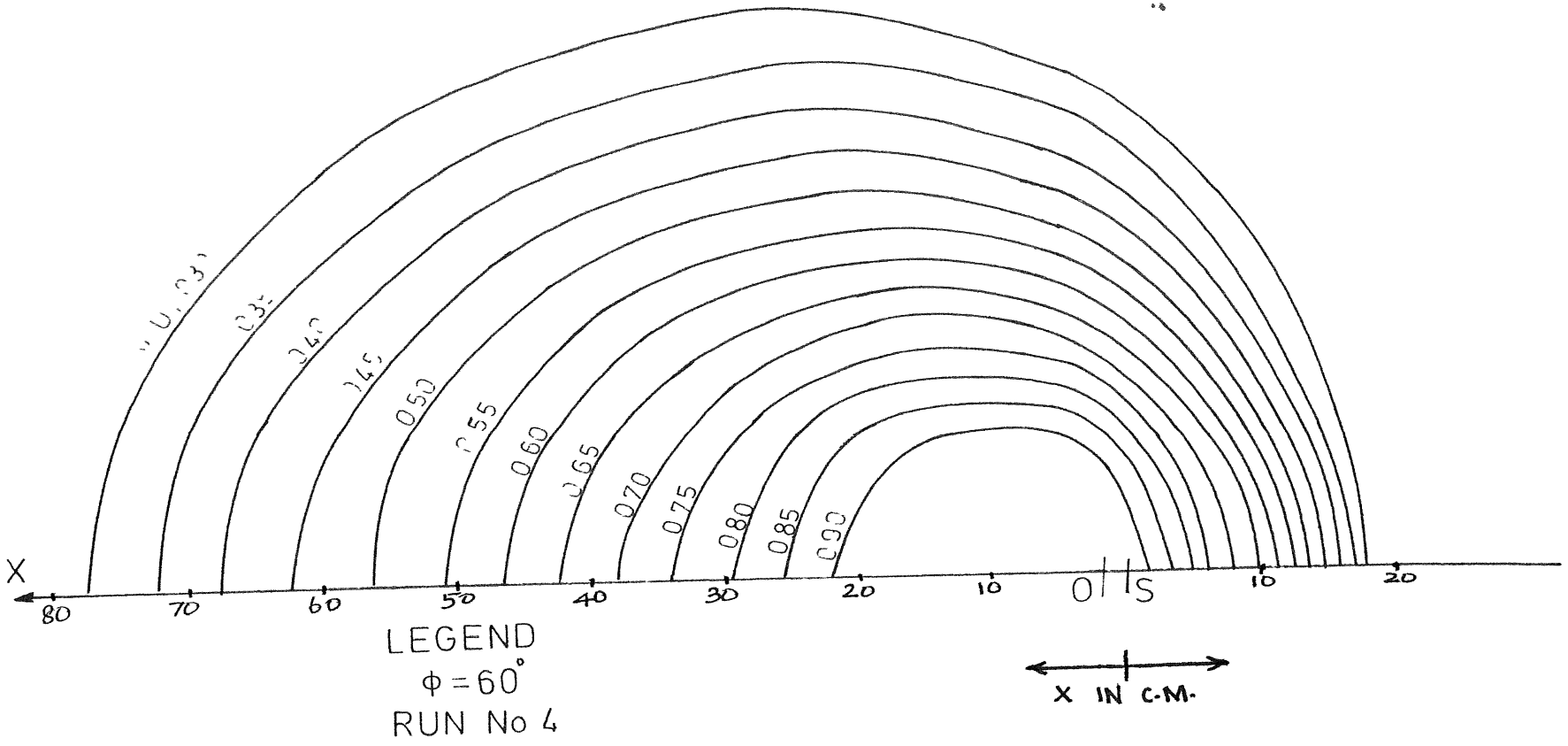

FIGURE 73 d MEAN VELOCITY CONTOURS

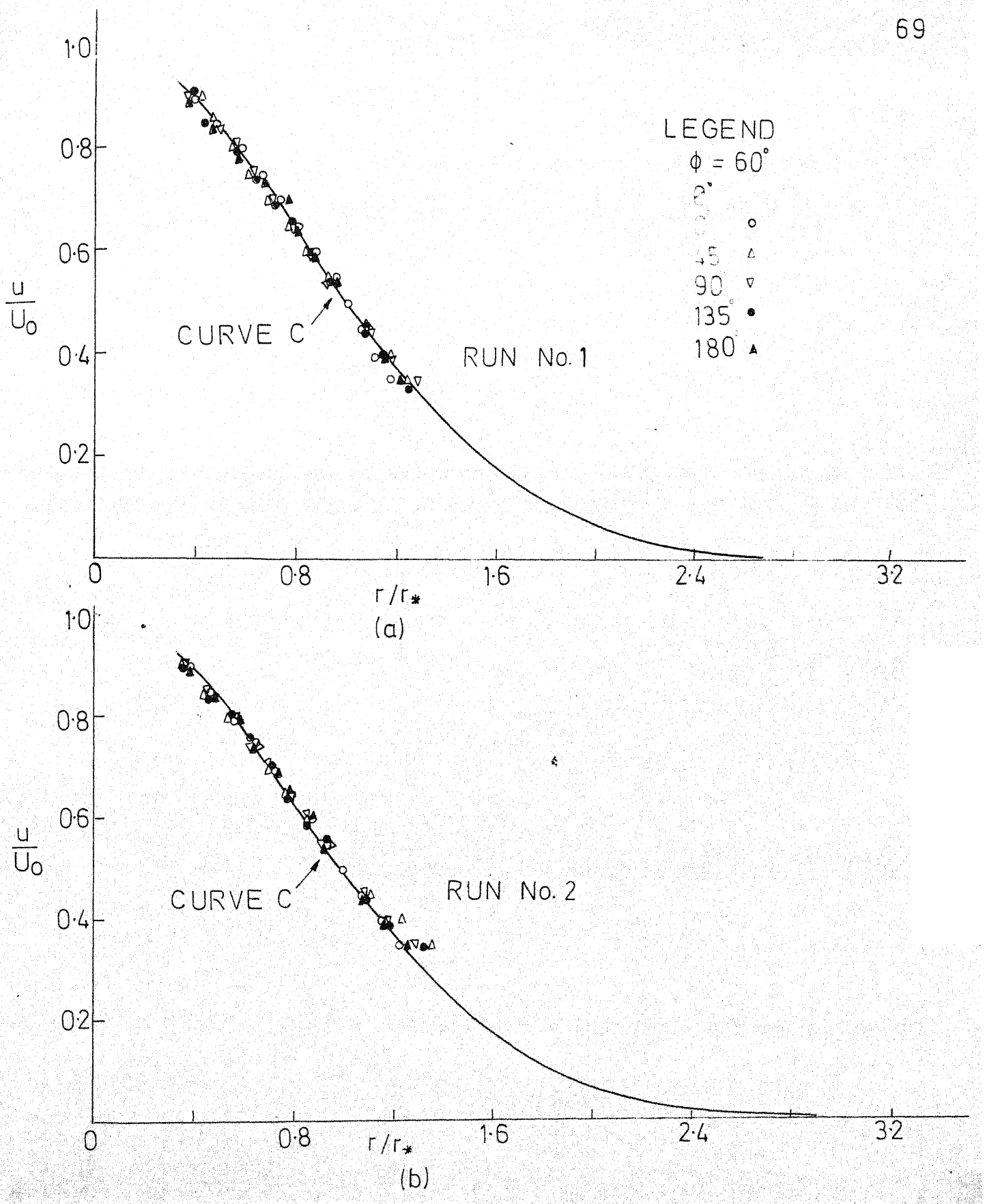

FIGURE 7·4 SIMILARITY MEAN VELOCITY PROFILES

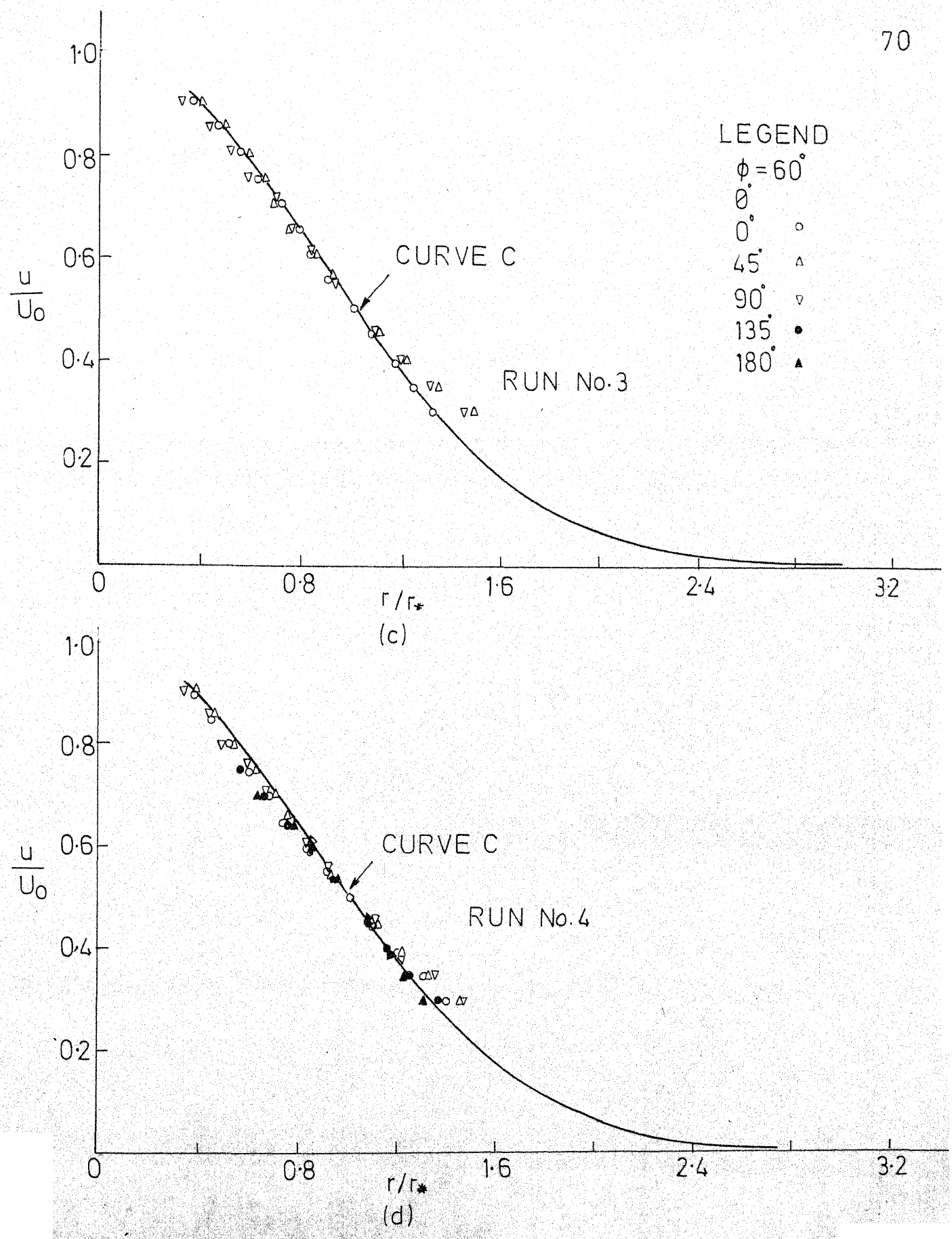

FIGURE 7·4 SIMILARITY MEAN VELOCITY PROFILES

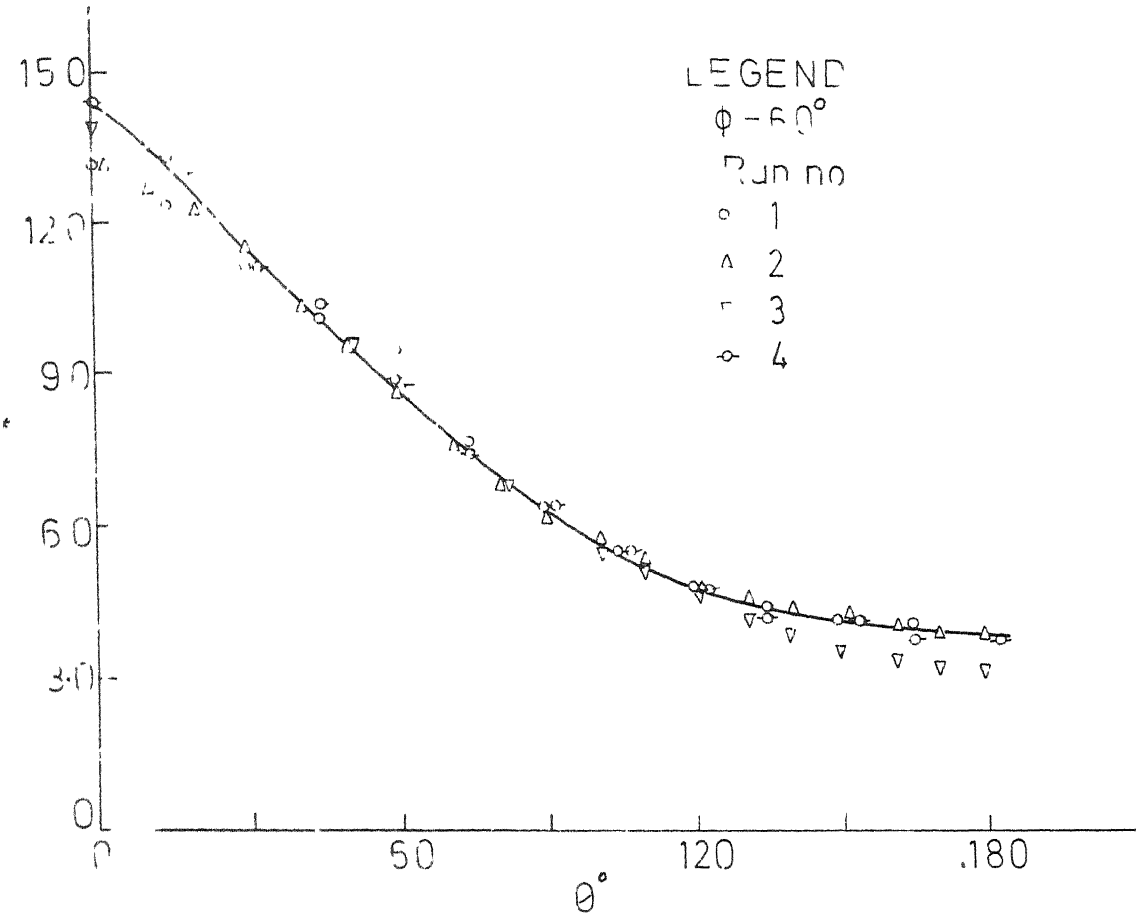

FIGURE 45 LENGTH SCALE PLOT

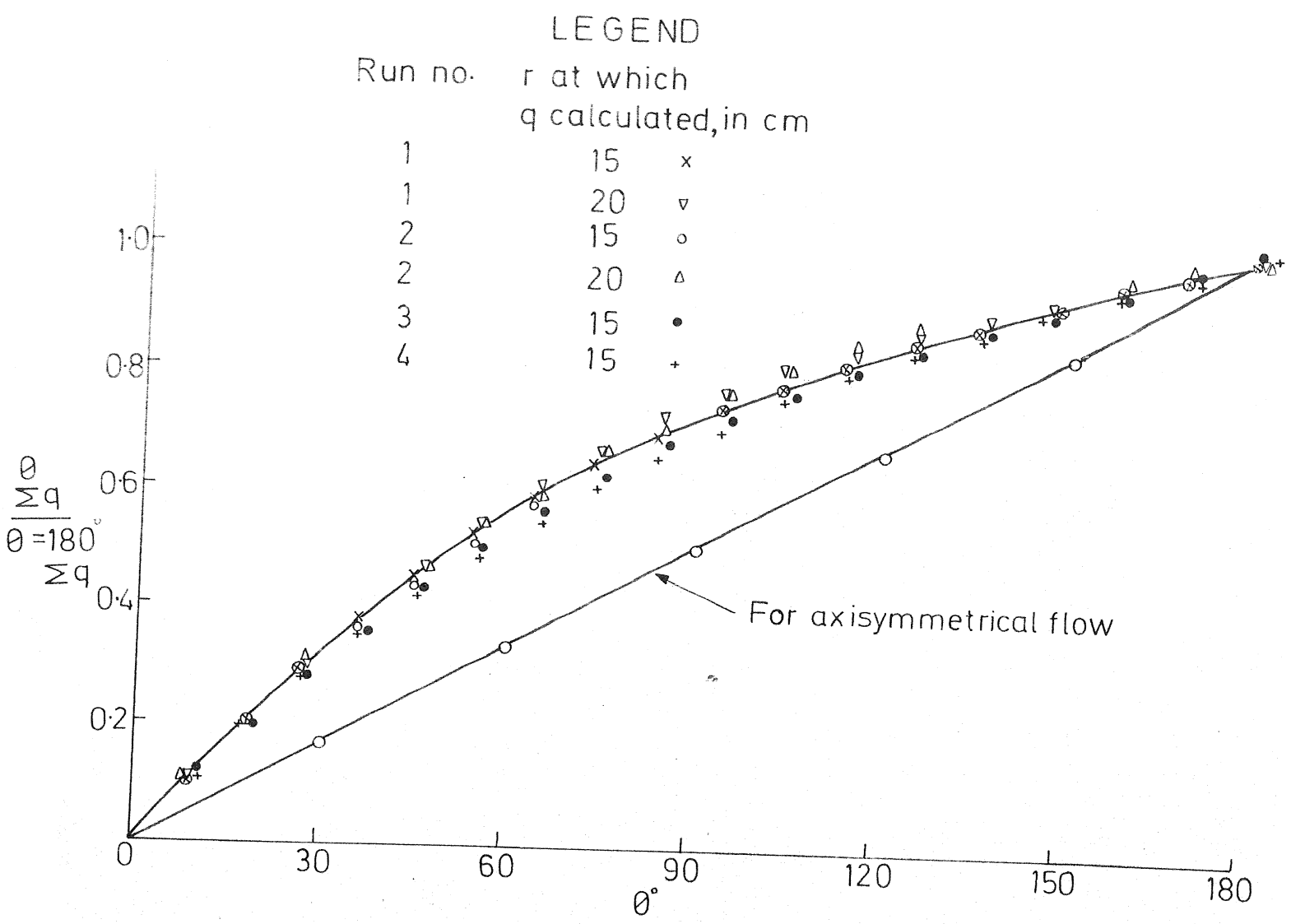

FIGURE 7·6 CUMULATIVE DISCHARGE VARIATION

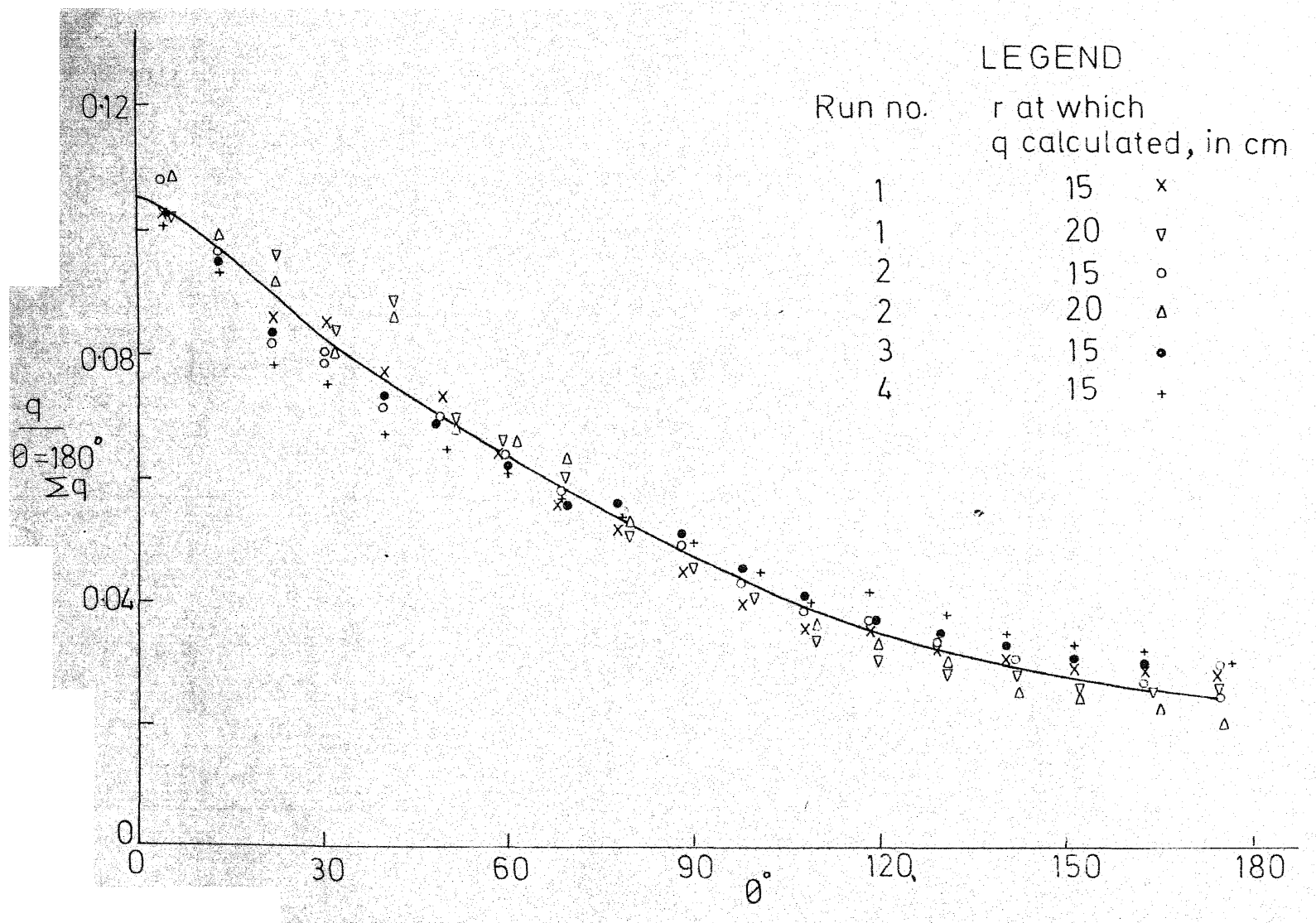

LEGEND

Run no.	r at which q calculated, in cm	
1	15	×
1	20	▽
2	15	○
2	20	△
3	15	●
4	15	+

FIGURE 7·7 DISCHARGE DISTRIBUTION

CHAPTER 8

CONCLUSIONS AND RECOMMENDATIONS

This exploratory study was aimed at to investigate the behaviour of free flow jet impingement on the plane surface. From the analysis and discussion the following conclusions can be drawn.

1. In the impingement region, along the radial lines studied, the non-dimensional pressure $\frac{P}{P_s}$ has got the same variation as in the case of submerged jet impingement irrespective of the nature of impingement and it can be expressed by the Gaussian equation as $\frac{P}{P_s} = \exp(-0.693\,\beta^2)$. However, the length scale, δ^* is smaller than that of corresponding submerged jet impingement.

2. The mean velocity profile along any radial direction can be expressed by the Gaussian equation as $\frac{u}{U_o} = \exp(-0.693\,\alpha^2)$, where $\alpha = \frac{r}{r_*}$.

3. The non-dimensional length scale $\frac{r_*}{d}$ is independent of U_o for a given ϕ and H/d.

4. The non-dimensionalised cumulative discharge variation $\frac{\Sigma q}{\theta=180^{\circ}}$ and the sector discharge variation $\frac{q}{\theta=180^{\circ}}$ is independent of U_o and d and dependent upon θ only for a given ϕ and H/d.

Recommendations:

The effects of change of ϕ, d and H is to be studied in all the flow regions in greater detail.

APPENDIX B-1

REFERENCES

1. ARBHABHIRAMA, A. and WAN, W.C., "Characteristics of a Circular Jump in a Radial Wall Jet", J. of Hydraulic Research, Vol. 13, No.3, 1975, pp. 239-262.

2. KOLOSEUS, H.J. and AHMAD, D., "Circular Hydraulic Jump", J. of Hyd. Div. Proc. ASCE, Vol.95, No. Hy1, January, 1969, pp. 409-422.

3. YAO, K.M., "Deflecting of a Circular Jet on a Plane Surface", Vishwakarma, A Journal of Engineering and Technology, Special number on symposium on Hydraulics and Hydraulic Machines, I.I.Sc., Bangalore, May, 1963, pp. 349-353.

APPENDIX B-2

ELECTRONIC WATER SENSOR

A simple circuit has been built to detect the water flow profile. The circuit is shown in the Figure, below and it consists of only two transistors and two resistors. Transistor Q_1 (BC157) is used as a sensor amplifier and Q_2 as a power amplifier for driving the indicator lamp when the probe just touches the water surface.

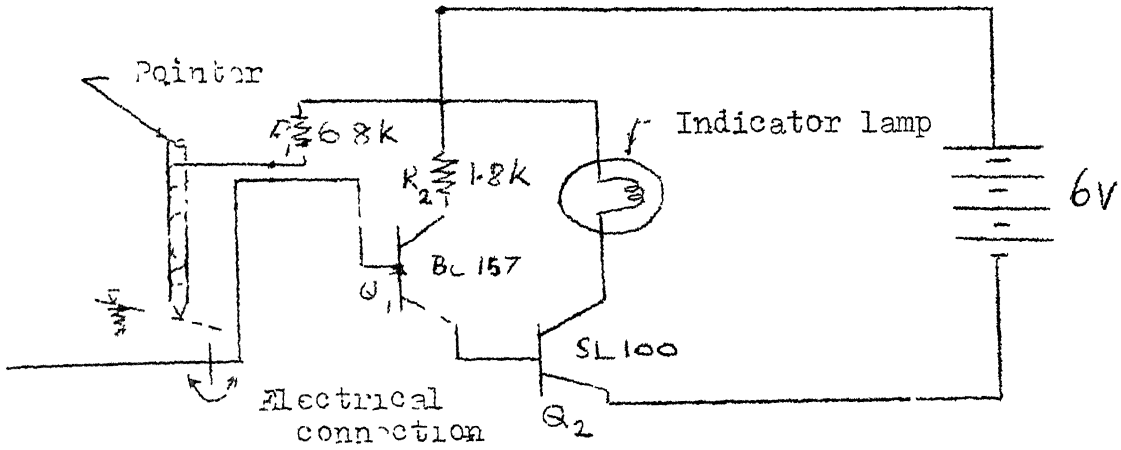

Q_1 - Transistor BC 157

Q_2 - Transistor SL 100

R_1 - Resistor 6.8K

R_2 - Resistor 1.8K

DEPTH AND VELOCITY MEASUREMENT DATA

RUN No.1

Radial Distance from G.C.	θ^{o}=0		30		60		90		120		150	
	Depth, y in cm.	Velocity, u in cm/sec.	Depth, y in cm.	Velocity, u in cm/sec.	Depth, y in cm.	Velocity, u in cm/sec.	Depth, y in cm.	Velocity, u in cm/sec.	Depth, y in cm.	Velocity, u in cm/sec.	Depth, y in cm.	Velocity, u in cm/sec.
1	2	3	4	5	6	7	8	9	10	11	12	13
5.0	1.46	443	1.12	447	0.90	453	0.67	447	0.41	447	-	-
10.0	0.78	440	0.68	437	0.43	452	0.40	417	0.29	425	-	-
15.0	0.61	424	0.52	428	0.36	442	0.29	404	0.25	357	-	-
20.0	0.47	411	0.40	421	0.32	394	0.24	358	0.20	294	0.16	272
25.0	0.47	396	0.35	380	0.30	371	0.22	278	0.20	230	0.16	201
30.0	0.37	381	0.32	352	0.30	325	0.21	256	0.16	183	0.16	140
35.0	0.37	369	0.30	331	0.26	288	0.21	201	-	-	-	-
40.0	0.37	342	0.30	300	0.25	258	0.21	178	-	-	-	-
45.0	0.36	328	0.30	280	0.24	239	0.21	144	-	-	-	-
50.0	0.35	290	0.30	234	0.24	220	-	-	-	-	-	-
55.0	0.34	272	0.30	221	0.24	188	-	-	-	-	-	-
60.0	0.33	258	0.30	205	-	-	-	-	-	-	-	-

Contd.....

RUN No. 2

1	2	3	4	5	6	7	8	9	10	11	12	13
5.0	1.35	535	1.25	532	0.91	544	0.64	524	0.36	542	-	-
10.0	0.82	520	0.60	537	0.53	515	0.40	485	0.30	505	0.26	481
15.0	0.65	505	0.47	517	0.39	485	0.30	469	0.26	438	-	-
20.0	0.53	485	0.36	501	0.34	454	0.25	408	0.21	357	0.21	320
25.0	0.45	467	0.35	465	0.29	443	0.24	349	0.21	280	0.17	234
30.0	0.41	452	0.32	436	0.27	411	0.21	297	0.21	221	0.16	177
35.0	0.39	432	0.28	408	0.26	334	0.21	239	0.21	188	-	-
40.0	0.38	408	0.29	389	0.26	294	0.21	198	0.19	160	-	-
45.0	0.36	378	0.28	349	0.23	262	0.21	153	-	-	-	-
50.0	0.33	349	0.28	307	0.23	251	0.21	140	-	-	-	-
55.0	0.31	325	0.27	280	0.22	217	-	-	-	-	-	-
60.0	0.30	294	0.24	251	-	-	-	-	-	-	-	-

Contd.....

Appendix B-3 contd....

RUN No. 3

1	2	3	4	5	6	7	8	9	10	11	12	13
5.0	0.98	792	0.73	792	0.47	811	0.39	780	0.26	795	0.23	728
10.0	0.56	774	0.42	767	0.32	794	0.22	657	0.20	639	0.19	542
15.0	0.41	748	0.34	761	0.27	714	0.21	602	0.19	493	-	-
20.0	0.35	728	0.31	714	0.26	634	0.18	493	0.18	400	0.18	313
25.0	0.35	672	0.29	657	0.23	528	0.18	371	0.17	297	0.17	217
30.0	0.33	626	0.28	551	0.22	450	0.18	290	0.17	208	-	-
35.0	0.32	578	0.27	500	0.21	384	0.18	230	-	-	-	-
40.0	0.30	532	0.24	452	0.20	343	-	-	-	-	-	-
45.0	0.28	458	0.24	401	0.20	297	-	-	-	-	-	-
50.0	0.27	427	0.24	376	0.20	251	-	-	-	-	-	-
55.0	0.26	376	0.24	290	-	-	-	-	-	-	-	-
60.0	0.26	357	0,24	273	-	-	-	-	-	-	-	-

Contd.....

Appendix B-3 contd...

RUN No. 4

1	2	3	4	5	6	7	8	9	10	11	12	13
5.0	0.93	919	0.75	929	0.54	931	0.36	919	0.34	875	-	-
10.0	0.54	897	0.44	908	0.33	915	0.24	869	0.20	759	0.20	700
15.0	0.40	880	0.31	897	0.25	859	0.24	667	0.20	601	0.17	570
20.0	0.34	805	0.28	829	0.24	686	0.21	614	0.19	475	-	-
25.0	0.30	761	0.26	728	0.23	602	0.19	509	0.17	319	-	-
30.0	0.27	728	0.25	657	0.21	524	0.20	396	0.17	266	-	-
35.0	0.26	679	0.24	594	0.19	454	0.18	337	-	-	-	-
40.0	0.25	611	0.23	515	0.20	401	0.18	246	-	-	-	-
45.0	0.25	542	0.23	475	0.19	319	-	-	-	-	-	-
50.0	0.25	493	0.23	432	0.18	269	-	-	-	-	-	-
55.0	0.25	454	0.23	354	0.18	234	-	-	-	-	-	-
60.0	0.24	416	0.21	319	-	-	-	-	-	-	-	-

CE-1970-M-PEN-SAI